DMD Fast Forward. Published on July 7, 2021 as DOI: 10.1124/dmd.120.000307
This article has not been copyedited and formatted. The final version may differ from this version.

Role of Epoxide Hydrolases and Cytochrome P450s on Metabolism of KZR-616, a First-in-Class Selective Inhibitor of the Immunoproteasome

Ying Fang, Henry Johnson, Janet L. Anderl, Tony Muchamuel, Dustin McMinn, Christophe Morisseau[1], and Bruce D. Hammock[1], Christopher Kirk, Jinhai Wang*,

Kezar Life Sciences, South San Francisco, CA 94080

[1]University of California, Davis, CA 95616

*Corresponding author: Jinhai Wang, Ph.D., jwang@kezarbio.com

Downloaded from dmd.aspetjournals.org at ASPET Journals on April 16, 2024

DMD Fast Forward. Published on July 7, 2021 as DOI: 10.1124/dmd.120.000307
This article has not been copyedited and formatted. The final version may differ from this version.

Running Title Page

Running title: Microsomal epoxide hydrolase on metabolism of KZR-616

Corresponding author: Jinhai Wang, Ph.D., Department of Drug Metabolism and Pharmacokinetics, Kezar Life Sciences, South San Francisco, CA 94080, jwang@kezarbio.com

Number of text pages: 38

Number of tables: 4

Number of figures:7

Number of schemes:1

Number of supplemental figures:3

Number of supplemental tables: 1

Number of references: 43

Number of words in the Abstract: 230

Number of words in the Introduction: 601

Number of words in the Discussion: 1328

Abbreviations

1-ABT:1-aminobenzotriazole; BSA: bovine serum albumin; CYP: cytochrome P450 Cl_{int}: intrinsic clearance; DDI: drug-drug interaction; FA: formic acid; HLM: human liver microsome; IS: internal standard; RA: rheumatoid arthritis; LC-MS/MS: liquid chromatography with tandem mass spectrometry; mEH: microsomal epoxide hydrolase; MLM: monkey liver microsome; MM: multiple myeloma; NSPA: 2-nonylsulfanyl-propionamide; PK: pharmacokinetics; SD: standard deviation; sEH: soluble epoxide

Downloaded from dmd.aspetjournals.org at ASPET Journals on April 16, 2024

DMD Fast Forward. Published on July 7, 2021 as DOI: 10.1124/dmd.120.000307
This article has not been copyedited and formatted. The final version may differ from this version.

hydrolase; *cis*-SO: *cis*-stilbene oxide; SLE: systemic lupus erythematosus; *trans-SO*: *trans*-stilbene oxide; TPPU:1-trifluoromethoxyphenyl-3-(1-propionypiperidin-4-yl) urea

Abstract

KZR-616 is an irreversible tripeptide epoxyketone-based selective inhibitor of the human immunoproteasome. Inhibition of the immunoproteasome results in anti-inflammatory activity *in vitro* and, based on promising therapeutic activity in animal models of rheumatoid arthritis (RA) and systemic lupus erythematosus (SLE), KZR-616 is being developed for potential treatment of multiple autoimmune and inflammatory diseases. The presence of a ketoepoxide pharmacophore presents unique challenges in the study of drug metabolism during lead optimization and clinical candidate profiling. This study presents a thorough and systematic *in vitro* and cell-based enzymatic metabolism and kinetic investigation to identify the major enzymes involved in the metabolism and elimination of KZR-616. Upon exposure to liver microsomes in the absence of NADPH, KZR-616 and its analogs were converted to their inactive diol derivatives with varying degrees of stability. Diol formation was also shown to be the major metabolite in pharmacokinetic studies in monkeys and correlated with *in vitro* stability results for individual compounds. Further study in intact hepatocytes revealed that KZR-616 metabolism was sensitive to an inhibitor of microsomal epoxide hydrolase (mEH) but not inhibitors of cytochrome P450 (CYP) or soluble epoxide hydrolase (sEH). Primary human hepatocytes were determined to be the most robust source of mEH activity for study *in vitro*. These findings also suggest that the exposure of KZR-616 *in vivo* is unlikely to be affected by co-administration of inhibitors or inducers of CYP and sEH.

Downloaded from dmd.aspetjournals.org at ASPET Journals on April 16, 2024

DMD Fast Forward. Published on July 7, 2021 as DOI: 10.1124/dmd.120.000307
This article has not been copyedited and formatted. The final version may differ from this version.

Significance Statement

This work presents a thorough and systematic investigation of metabolism and kinetics of KZR-616 and related analogs in *in vitro* and cell-based enzymatic systems. Information gained could be useful in assessing novel covalent proteasome inhibitors during lead compound optimization. These studies also demonstrate a robust source *in vitro* test system that correlated with *in vivo* PK for KZR-616 and 2 additional tripeptide epoxyketones.

Downloaded from dmd.aspetjournals.org at ASPET Journals on April 16, 2024

DMD Fast Forward. Published on July 7, 2021 as DOI: 10.1124/dmd.120.000307
This article has not been copyedited and formatted. The final version may differ from this version.

Introduction

The proteasome has been validated as a therapeutic drug target through regulatory approval of 3 compounds for use in the treatment of B-cell neoplasms, such as multiple myeloma and mantle cell lymphoma (Bross et al., 2004; Kisselev et al., 2012; Herndon et al., 2013). These compounds comprise 2 chemical classes: the reversible boronic acid derivatives, bortezomib (VELCADE®) and ixazomib (NINLARO®), and the tetrapeptide epoxyketone-based compound, carfilzomib (Kyprolis®). Unlike bortezomib and ixazomib, carfilzomib is the first of a new generation of irreversible inhibitors that target proteasome subunits with prolonged inhibition and high selectivity (Demo et al., 2007; Kapur et al., 2011). Validated with the success of 3 approved agents, next generation proteasome inhibitors are now an important class of drugs being investigated for other diseases (Teicher and Tomaszewski, 2015).

The immunoproteasome is a unique form of proteasome mainly expressed in immune effector cells (Miller et al., 2013). The immunoproteasome distinguishes itself from the ubiquitously-expressed constitutive proteasome by the presence of 3 distinct catalytic subunits: LMP7 (low-molecular mass polypeptide-7), LMP2 and MECL-1 (multi-catalytic endopeptidase complex-like 1). These active site subunits can also be induced in non-immune cells upon exposure to inflammatory cytokines such as tumor necrosis factor alpha (TNF-α) or interferon gamma (IFN-γ) (Deborah et al., 2012). Selective inhibition of the immunoproteasome results in a reduction of inflammatory cytokines from immune effector cells and can block disease progression in animal models of several autoimmune diseases including rheumatoid arthritis (RA), multiple sclerosis, and systemic lupus erythematosus (SLE) (Puttaparthi et al., 2005; Egerer et al., 2006;

Downloaded from dmd.aspetjournals.org at ASPET Journals on April 16, 2024

Groettrup 2010; Basler and Groettrup, 2012; Miller et al., 2013; Basler et al., 2015). KZR-616 (Figure 1) is a tripeptide epoxyketone which selectively and irreversibly inhibits the LMP7 and LMP2 subunits of the human immunoproteasome; it was selected for clinical development following a thorough medicinal chemistry campaign (Johnson et al., 2018). In human peripheral blood mononuclear cells (PBMC), KZR-616 blocks inflammatory cytokine production, including TNF-α, granulocyte-macrophage colony-stimulating factor (GM-CSF), interleukin (IL)-6, and IL-23. In lymphocytes, T-cell production of IFN-γ, TNF-α and GM-CSF and differentiation of activated B-cells to plasma blasts are inhibited by KZR-616 (Muchamuel et al., 2017). Finally, in mouse models of RA and SLE, KZR-616 blocks disease progression at well-tolerated doses without affecting normal T-cell-dependent immune responses (Muchamuel et al., 2017; Johnson et al., 2018). KZR-616 is currently being evaluated in Phase 2 clinical trials in patients with SLE and lupus nephritis.

Like carfilzomib, KZR-616 is an exquisitely chemo-selective, irreversible covalent inhibitor of N-terminal threonine proteases, a class of proteases to which the proteasome active site subunits are nearly exclusive (Kisselev et al., 2012). While the boronic acid-based proteasome inhibitors were shown to have a primary metabolic pathway involving oxidation via classical Phase 1 cytochrome P450 (CYP) enzymes, carfilzomib is believed to be cleared extrahepatically via peptidase cleavage and epoxide hydrolysis to an inactive diol (Yang et al., 2011; Wang et al., 2013). Oprozomib, a tripeptide epoxyketone analog of carfilzomib, which is currently under clinical investigation in multiple myeloma, was shown to be a substrate of microsomal epoxide hydrolase (mEH) (Wang et al., 2017). Given the structural similarities between KZR-616 and both

Downloaded from dmd.aspetjournals.org at ASPET Journals on April 16, 2024

DMD Fast Forward. Published on July 7, 2021 as DOI: 10.1124/dmd.120.000307
This article has not been copyedited and formatted. The final version may differ from this version.

carfilzomib and oprozomib, we aimed to determine the major and specific metabolic pathways and enzymes involved in metabolism of KZR-616 prior to initiation of clinical trials in chronic disorders. In addition, by conducting a thorough and methodical *in vitro* experimental approach and assessing pharmacokinetics in large animals, we were able to carry out *in vitro* to *in vivo* extrapolation (IVIVE) correlations to determine which surrogate absorption, distribution, metabolism and excretion (ADME) *in vitro* model system is most informative for development of novel epoxyketone-based clinical candidates.

Downloaded from dmd.aspetjournals.org at ASPET Journals on April 16, 2024

DMD Fast Forward. Published on July 7, 2021 as DOI: 10.1124/dmd.120.000307
This article has not been copyedited and formatted. The final version may differ from this version.

Materials and Methods

Materials and cell growth conditions All chemicals and reagents were obtained from Sigma (St. Louis, MO) and liquid chromatography (mass spectrometry (MS) grade) solvents were obtained from Fisher Scientific (Pittsburgh, PA). KZR-616, deuterated KZR-616 (d_8-KZR-616), KZR-59587, KZR-59177, KZR-59240 and KZR-616 analogs were synthesized at Kezar Life Sciences. 2-Nonylsulfanyl-propionamide (NSPA), human recombinant mEH and soluble epoxide hydrolase (sEH) were gifts from Bruce Hammock's lab at the University of California, Davis (Morisseau et al., 2008; Newman et al., 2003). 1-Trifluoromethoxyphenyl-3-(1-propionylpiperidin-4-yl) urea (TPPU) and 1-aminobenzotriazole (1-ABT), were obtained from Sigma. Liver subcellular fractions including male or female monkey liver microsomes (pool of 6; 20 mg/mL), cytosols (pool of 6; 10 mg/mL), human liver subcellular fractions including male or female liver microsomes (pool of 10, 20 mg/mL), cytosols (mixed gender; pool of 50, 10 mg/mL), pooled human cryopreserved hepatocytes (100 donors, mixed gender) and culture media (K8400) and monkey cryopreserved hepatocytes (5 donors of male cynomolgus monkey, PPCH 2000) and culture media (20-1-0526) were purchased from Sekisui Xenotech (Kansas City, KS). Human hepatocytes were incubated at 37°C in an environment of 95% air/5% CO_2.

Metabolic stability in liver microsomes (LM) in the presence and absence of nicotinamide adenine dinucleotide phosphate (NADPH) Reactions were assessed in pooled human (H) and monkey (M) LM with or without NADPH. Test compound and probe substrates were mixed with HLM (0.5 mg/mL) and MLM (0.25 mg/mL) with or without 1.2 mM NADPH in 0.1 M potassium phosphate buffer (pH 7.4) containing 3.3

Downloaded from dmd.aspetjournals.org at ASPET Journals on April 16, 2024

DMD Fast Forward. Published on July 7, 2021 as DOI: 10.1124/dmd.120.000307
This article has not been copyedited and formatted. The final version may differ from this version.

mM $MgCl_2$. Mixtures were kept at 37°C for up to 60 minutes and reactions were terminated at indicated timepoints by addition of 2 volumes of acetonitrile containing 0.1% formic acid (FA) and 25 nM of internal standard (IS) d_8-KZR-616. The disappearance of test compound and their diol metabolites, and the metabolites of probe substrates were monitored using liquid chromatography with tandem mass spectrometry (LC-MS/MS) or liquid chromatography with ultraviolet detection (LC-UV) methods as described below. Each experimental reaction was conducted in triplicate. The intrinsic clearance (Cl_{int}) was displayed by the rate of parent compound disappearance. Testosterone (50 µM) and *cis*-stilbene oxide (*cis*-SO; 50 µM) were used as probe substrates for CYP and mEH, respectively.

Metabolic stability in monkey hepatocytes Pooled cryopreserved monkey hepatocytes were thawed and re-suspended in culture media. KZR-59177, KZR-616 and KZR-59240 (1 µM) and reference substrates (50 µM testosterone, *cis*-SO and *trans*-SO) were incubated in duplicate with monkey hepatocytes (0.25 x 10^6 cells/mL) in a 37°C cell culture incubator with 95% air and 5% CO2 for 40 min. Reactions were terminated at various timepoints by addition of 2 volumes of acetonitrile containing 0.1% FA and 25 nM of IS d_8-KZR-616. Samples were centrifuged, and KZR-616, KZR-59177, KZR-59240, their diol metabolites KZR-59587, KZR-59165, KZR-59433, and the metabolites of probe substrates were quantified by LC-MS/MS and LC-UV as described below. Testosterone (50 µM), *cis*-stilbene oxide (*cis*-SO; 50 µM), and *trans*-stilbene oxide (*trans*-SO; 50 µM) were used as probe substrates for CYP and EH, respectively.

CYP phenotyping in LM KZR-616 was incubated in HLM in the absence and presence of known chemical inhibitors for the six major CYP isoforms: furafylline (CYP1A2, 10

Downloaded from dmd.aspetjournals.org at ASPET Journals on April 16, 2024

μM), montelukast (CYP2C8, 5 μM), sulfaphenazole (CYP2C9, 5 μM), benzylnirvanol (CYP2C19, 1 μM), quinidine (CYP2D6, 1 μM) and ketoconazole (CYP3A4/5, 1 μM). Reaction mixtures contained a final concentration of 1 μM KZR-616, 0.2 mg/mL HLM protein, and 1 mM NADPH in 100 mM potassium phosphate, pH 7.4 buffer with 3.3 mM $MgCl_2$. The extent of metabolism was calculated as the disappearance of KZR-616 after incubation of 15, and 30 min, compared to the 0-min control reaction incubations. The formation of KZR-59587 (KZR-616 diol) was monitored, as well.

Liver microsome binding MLM (0.25 mg/mL) and HLM (0.5 mg/mL) were pre-incubated with 50 μM of NSPA in 0.1 M potassium phosphate buffer (pH 7.4) for 10 min followed by addition of KZR-616, KZR-59177, KZR-59240, and Chlorpromazine (control) at a final concentration at 1 μM and incubation at 37°C for 30 min. Incubated solutions were centrifuged at 85,000 rpm for 4 h at 37ºC and aliquots (30 μL) of the supernatants were added with equal volume of compound-free blank LM residues and aliquots (30 μL) of the LM residues were added with equal volume of compound-free blank supernatants. Samples were quenched with 150 μL of internal standard solution in acetonitrile/methanol (1:1) containing 0.1% FA. After centrifugation, the supernatants of all samples were subjected to LC-MS/MS analysis. The percentage of test compound bound to protein is calculated by the following equation: % Free = (concentration of the test compound in supernatant/concentration of the test compound in LM residues) × 100%; % Bound test compound = 100% - % Free

Plasma protein binding. KZR-616 binding to cynomolgus monkey plasma binding was conducted by equilibrium dialysis. Dialysis plates were prepared by adding 350 μL phosphate buffer (pH7.4) to the buffer chamber and 200 μL of 5 μM KZR-616 and

Downloaded from dmd.aspetjournals.org at ASPET Journals on April 16, 2024

controls (phenacetine; quinidine and warfarin) to the Red side. The plates were sealed and incubated at 37°C for 5 h at 100 rpm on an orbital shaker. Duplicate analysis samples were prepared by mixing 50 µL plasma sample (from Red side) with 50 µL of blank buffer and 50 µL buffer sample (from buffer chamber) with 50 µL of blank plasma. Samples were quenched with 150 µL of internal standard solution in acetonitrile/methanol (1:1) containing 0.1% FA. After centrifugation, the supernatants of all samples were subjected to LC-MS/MS analysis.

Pharmacokinetics (PK) in monkeys All of the animal studies were carried out in accordance with the Guide for the care and use of Laboratory Animals as adopted and promulgated by the US National Institutes of Health, and were approved by the Institution's Animal Care and USE Committee or local equivalent (Institute of Laboratory Animal resources, 1996). KZR-616, KZR-59177 and KZR-59240 were administrated to cynomolgus monkeys as single subcutaneous (SC) administrations. A total of 16 male, non-naïve and non-fasted animals were randomly divided into 3 groups (4 animals/group) receiving a dose of 3 mg/kg of the test compounds in aqueous 10% polysorbate (PS-80). Blood samples were collected prior to dosing, and at 2, 5, 10, 20 and 30 min, and 1, 2, 4, 8 and 24 h post dose. Plasma samples were obtained by centrifuging at 3,000 rpm at 4°C for 5 minutes. Plasma samples were quenched by addition of 3 volumes of acetonitrile containing 0.1% FA and 25 nM of IS d_8-KZR-616. Parent and diol metabolite levels were quantified by LC-MS/MS as described below.

Metabolism via recombinant human EH Reactions were conducted in 0.1 M Tris-HCl buffer for mEH (pH 9.0) and sEH (pH 7.5) containing 0.1 mg/mL fatty acid-free bovine serum albumin (BSA). A series of enzyme incubation solutions was pre-warmed for 5

Downloaded from dmd.aspetjournals.org at ASPET Journals on April 16, 2024

min at 37°C before the addition of 1 µM carfilzomib or KZR-616. Enzyme concentrations were 2, 4, 8 and 10 µg/mL for mEH, and 1, 10, 25, 50, and 100 µg/mL for sEH. Reactions were terminated after 60 min by addition of 2 volumes of acetonitrile containing 0.1% FA and 25 nM of IS d_8-KZR-616. Diol formation was quantified by LC-MS/MS. *Trans*-stilbene oxide (*trans*-SO, 50 µM) and *cis*-SO (50 µM) were used as probe substrates for sEH and mEH, respectively, and diol formation was quantified by LC-UV as described below.

Metabolic profiling of KZR-616 in human hepatocytes

Pooled cryopreserved human hepatocytes were thawed and re-suspended in cell culture media Reactions containing hepatocytes (2 x 10^6 cells/mL) and KZR-616 (10 µM) were conducted in cell media in a 24 well cell culture plate at a 37°C cell culture incubator with 95% air and 5% CO_2 for 2 hours. Reactions were terminated by addition 4 volumes of acetonitrile containing 0.1% FA. A separate aliquot of hepatocytes (2x10^6 cells/mL) was quenched with 4 volumes of acetonitrile, and then spiked with KZR-616 (10 µM) as a control sample. The resulting mixture was centrifuged at 4,000 rpm for 15 min. Supernatants were dried under a N_2 stream and the resultant residue was reconstituted with 30% acetonitrile (v/v) before LC-MS/MS analysis. Metabolite identification was conducted using an Applied Bio-systems mass spectrometer (API 4000 QTrap) with Shimadzu LC-20. Chromatographic separation was performed using a Kinetex 2.6 µ C18 100A column (3.0 mm × 50 mm) with mobile phases (A: water containing 0.1% FA; B: acetonitrile containing 0.1% FA) at a flow rate of 0.6 mL/min. The mobile phase step increased from 5% (at 0.3 min) to 95% B (at 12 min). The total run time was 15 min.

Downloaded from dmd.aspetjournals.org at ASPET Journals on April 16, 2024

DMD Fast Forward. Published on July 7, 2021 as DOI: 10.1124/dmd.120.000307
This article has not been copyedited and formatted. The final version may differ from this version.

Metabolism in human hepatocytes Pooled cryopreserved human hepatocytes (0.5 x 10^6 cells/mL) were pre-incubated in culture media (containing 0.1% dimethyl sulfoxide (DMSO) with varying concentrations of inhibitors of EHs or CYP (10 µM NSPA for 5 min; 200 µM TPPU and 500 µM 1-ABT for 30 min) in a 37°C cell culture incubator with 95% air and 5% CO_2. After pre-incubation, KZR-616 (1 µM) and reference substrates (50 µM testosterone, *cis*-SO and *trans*-SO) were incubated in triplicate in the presence or absence (1-ABT, NSPA and TPPU respectively in a 37°C cell culture incubator for 1 hour. After 1, 10, 20, 30, 40, and 60 min as indicated, reactions were terminated by addition of 2 volumes of acetonitrile containing 0.1% FA and 25 nM of IS d_8-KZR-616. Samples were centrifuged, and KZR-616, the diol and metabolites of reference substrates were quantified by LC-MS/MS and LC-UV as described below.

Metabolite profiling of KZR-616 in human plasma

Plasma samples were collected from patients with systemic lupus erythematous (SLE) receiving weekly subcutaneous administration of KZR-616 for 13 weeks (NCT03393013). Samples from patients receiving a KZR-616 dose of 75 mg, the maximum administered dose, were analyzed. Each sample was AUC pooled from the time points of blood withdraw (pre-dose, 0.0833, 0.25, 0.5, 1, 2, 4, 8 h post dose) on day 29 from one of the four subjects (110-004, 112-021, 113-002 and 116-012). Each plasma sample (400 µL) was extracted with 3 volumes of ACN/MeOH (1:1) containing 0.1% FA, and then centrifuged at 3,000 rpm for 15 min. The supernatant from each sample was concentrated under a nitrogen stream and reconstituted in 200 µL of 30% ACN/MeOH (1:1) containing 0.1% FA. Each sample was injected into the LC-MS system for separation and identification. Chromatographic separation was performed using a Waters

Downloaded from dmd.aspetjournals.org at ASPET Journals on April 16, 2024

XBridge C18, 3.0 x 150 mm, 3.5 µm with mobile phases (A: water containing 0.1% FA; B: acetonitrile containing 0.1% FA) at a flow rate of 0.8 mL/min. The mobile phase step increased from 3% at 0.3 min to 35% B at 25 min and to 90 % B at 26 min. The total run time was 35 min. Metabolite identification was conducted using an AB Sciex Triple TOF API6600™ mass spectrometer equipped with a Shimadzu Nexera™ UPLC system. Metabolite structures were assigned based on accurate mass (±5 mDa) determination of a parent ion from a full-scan TOF MS followed by triggered MS/MS fingerprints.

Reaction kinetics Reaction kinetics of KZR-616 were conducted in female and male HLM (0.5 mg/mL) and MLM (0.2 mg/mL) in 0.1 M potassium phosphate buffer (pH 7.4) with 0.1 mg/mL BSA at 37°C for 30 min. The kinetics of KZR-616 were also studied in human hepatocytes in hepatocyte maintenance medium at 37°C for 30 min. Reaction kinetics of KZR-616 were determined in 4 µg/mL recombinant human mEH at 37°C for 30 min in 0.1 M Tris-HCl buffer (pH 9.0) containing 0.1 mg/mL BSA. After pre-warming enzymes for 5 min, KZR-616 (0-1000 µM) was added to initiate the reaction. For kinetic study of carfilzomib, incubations were optimized and conducted using 2 µg/mL pre-warmed recombinant human mEH at 37°C for 20 min in 0.1 M Tris-HCl buffer (pH 9.0) containing 0.1 mg/mL BSA.

NSPA was assessed in female and male HLM (0.5 mg/mL) and MLM (0.25 mg/mL), human hepatocytes (0.5 x 10^6 cells/mL) and recombinant human mEH (4 µg/mL) to determine 50% inhibitory concentration (IC_{50}) values on KZR-616 (10 µM) utilizing varying concentrations of NSPA (0 to 100 µM) in the reaction buffers of the enzymes at 37°C for 15-30 min. NSPA was also assessed in recombinant human mEH to determine the IC_{50} on carfilzomib epoxide hydrolysis. Briefly, pre-warmed recombinant

Downloaded from dmd.aspetjournals.org at ASPET Journals on April 16, 2024

DMD Fast Forward. Published on July 7, 2021 as DOI: 10.1124/dmd.120.000307
This article has not been copyedited and formatted. The final version may differ from this version.

human mEH (2 µg/mL) was incubated with 1 µM CFZ in a range of NSPA concentrations (0-10 µM) at 37°C for 20 min. Reactions were terminated by addition of 2 volumes of acetonitrile containing 0.1% FA and 25 nM of IS d_8-KZR-616, and the concentrations of diol derivatives of KZR-616 and carfilzomib were quantified using LC-MS/MS methods. Each set of data was fit to a simple Michaelis-Menten kinetics model using nonlinear regression data analysis (GraphPad Prism 7.04.). Each experimental reaction was conducted in duplicate. *Cis*-SO (50 µM) incubation was conducted in parallel as a positive control.

Epoxide hydrolase inhibition activity In vitro inhibition potential of KZR-616 on mEH and sEH was investigated in LM and recombinant EH. *Cis*-SO and *trans*-SO were used as probe substrates for mEH and sEH, respectively. For testing of KZR-616 as an inhibitor of mEH, pre-warmed pooled HLM (0.5 mg/mL), MLM (0.25 mg/mL), and recombinant mEH (4 µg/mL) were incubated with *cis*-SO (50 µM) in the absence or presence of 100 µM KZR-616 in the reaction buffers at 37°C for 30 min. For study of KZR-616 as an inhibitor of sEH, pre-warmed pooled human hepatic cytosol (0.5 mg/mL) and recombinant sEH (100 µg/mL) were incubated with *trans*-SO (50 µM) in the absence or presence of 100 µM KZR-616 in 0.1 M potassium phosphate buffer (pH 7.4) containing 0.1 mg/mL BSA and in 0.1 M Tris-HCL buffer (pH 7.4) containing 0.1 mg/mL BSA, respectively. Reactions were quenched with 2 volumes of cold acetonitrile, and the concentrations of diol derivatives of *cis*-SO and *trans*-SO were quantified by using LC-UV methods as described below.

LC-MS/MS and LC-UV quantification LC-MS/MS methods were developed for quantifying carfilzomib, KZR-616, KZR-59177, KZR-59240, the CYP probe substrate

Downloaded from dmd.aspetjournals.org at ASPET Journals on April 16, 2024

(testosterone) and their diol derivatives using an AB Sciex 5500 Q-Trap mass spectrometer equipped with an electrospray ionization source. Multiple reaction monitoring was used with following mass transitions for each compound m/z (parent > product ion): 587.4>371.2, 605.1>389.2, 571.3>389.6, 589.7>150.1, 607.3>391.2, 719.8>402.2, 737.9>402.2, 289.3>109.1, 305.1>269.1, and 594.9>371.2 for KZR-616, KZR-59587 (diol), KZR-59177, KZR-59165 (diol), KZR-59240, KZR-59433 (diol) carfilzomib, testosterone, 6β-testosterone, and IS d_8-KZR-616, respectively. Chromatographic separation was achieved using YMC-pack pro C18 (3 µ, 3.0 mm × 50 mm) (A)-water and (B)-acetonitrile containing 0.1% FA at flow rate of 0.5 and 1.0 mL/min. For the flow rate at 0.5 mL/min, the mobile phase started at 5% B for 0.5 min, and progress linearly to 95% acetonitrile in 2.3 min, hold at 95% B for 0.7 min and returned to 5% B with 0.1 min. For the flow rate at 1.0 mL/min, the mobile phase started at 10% B for 0.5 min, followed by a linear change up 95% acetonitrile in 1.7 min, hold at 95% B for 0.5 min and returned to 5% B with 0.1 min.

Quantification of *cis*-SO, *trans*-SO and corresponding metabolites was fulfilled using a LC-30AD system coupled with a SPD-20AV detector. Chromatographic separation was achieved using Kinetex reverse phase C18 (1.7 µ, 2.1 mm × 50 mm) column with mobile phase (A)-water and (B)-acetonitrile containing 0.1% FA at flow rate of 0.5 mL/min. The mobile phase started at 10% B for 1.0 min, and gradually increased to 95% acetonitrile in 5 min, hold at 95% B for 1.0 min and returned to 10% B with 0.1 min.

A calibration curve was established for each test compound by plotting its peak area ratio for each compound against IS (d8-KZR-616) versus the corresponding concentrations of each compound across a calibration range (1 to 5000 ng/mL), and

Downloaded from dmd.aspetjournals.org at ASPET Journals on April 16, 2024

DMD Fast Forward. Published on July 7, 2021 as DOI: 10.1124/dmd.120.000307
This article has not been copyedited and formatted. The final version may differ from this version.

fitting with a linear regression equation. The calibration curve was then used to calculate the concentration of each test compound.

Kinetic analysis and IC_{50} data processing

The kinetics of epoxide hydrolysis of KZR-616 were obtained from duplicate experiments with KZR-616 in a concentration range from 0 to 1000 µM. Km and Vmax were calculated by fitting the diol (KZR-59587) formation data into the Michaelis-Menten equation using GraphPad Prism software. IC_{50} was calculated by using nonlinear fit of log (inhibitor) versus response – variable slope. The IC_{50} data was validated only when the data lie within the inhibitor concentration range.

Statistical analysis GraphPad Prism was used for the statistical analysis. All data is expressed in mean ± S.D. format. For the kinetic and IC50 analyses, 95% CI (confidence interval) threshold with Goodness of Fit (R squared > 0.99) were used.

Downloaded from dmd.aspetjournals.org at ASPET Journals on April 16, 2024

DMD Fast Forward. Published on July 7, 2021 as DOI: 10.1124/dmd.120.000307
This article has not been copyedited and formatted. The final version may differ from this version.

Results

Characterization of the metabolism of KZR-616 and its analogs in liver microsomes and monkey hepatocytes

KZR-616 was selected from a medicinal chemistry effort that involved the synthesis of over 400 hundred tripeptide epoxyketones (patents: McMinn D, et al. Patent Appl. US9657057B2; Patent Appl. US10647744B2). To further understand the structure-activity relationship of this chemotype, the metabolic stability of a subset of 79 potent and selective analogs was evaluated in an *in vitro* model system utilizing HLM and MLM, which exhibit high levels of both mEH and CYP activity. Testosterone, *cis*-SO and *trans*-SO were used as probe substrates for CYP (Supplemental Figure 1), mEH and sEH (Supplemental Figure 2), respectively. Epoxide hydrolase stability was assessed in mixtures of compound and LM in the absence of NADPH to prevent CYP activity. As shown in Figure 2A, a wide range of epoxide hydrolysis stability across the 79 tested compounds was noted in both HLM and MLM incubations. KZR-616, KZR-59177 (an unstable analog) and KZR-59240 (a stable analog) were chosen as tool compounds to explore CYP-mediated metabolism pathways in LM. The intrinsic clearance of KZR-616, KZR-59177 and KZR-59240 increased significantly with the addition of NADPH in the LM incubations, suggesting that CYP enzymes play the dominant role in metabolism in this experimental system (Table 1).

We next determined the effect of microsomal binding on the intrinsic clearance rates of three test compounds. The % bound average was found to be 7.4 % and 12.3 % for KZR-616, and 21.3 % and 20.4 % for KZR-59240 in monkey and human LM mixtures, respectively. The % bound average for KZR-59177 was not applicable due to stability

Downloaded from dmd.aspetjournals.org at ASPET Journals on April 16, 2024

issues in the LM mixtures that led to negative % bound values. Overall, the difference of the % bound values between KZR-616 and KZR-59240 was small in respective human and monkey LM and, as such, the intrinsic clearance of KZR-616 and KZR-59240 (Table 1) can be considered reliable.

To evaluate the metabolic stability of these 3 compounds, we also selected cell-base *in vitro* model using monkey hepatocytes, which exhibit high levels of both mEH and CYP activity. As shown in Figure 2b, quantification of disappearance of KZR-59177, KZR-616, and KZR-59240 and their diol formations were performed using synthesized standards. The recovery of parents and diols were 82.0, 96.4, and 100% for KZR-59177, KZR-616, and KZR-59240, respectively, after 40 min incubations. These quantitative results suggest that epoxide hydrolysis was the major metabolic pathway for the 3 tool compounds in monkey hepatocytes.

CYP phenotyping demonstrated that CYP3A4/5 was the major enzyme involved in the microsomal metabolism of KZR-616, with CYP2C8 playing a minor role in its metabolism. Formation of the KZR-616 diol, KZR-59587, was not affected by the presence of CYP inhibitors, demonstrating that other enzymes, such as epoxide hydrolases, play important roles in diol formation (Supplemental Table1).

Pharmacokinetics of KZR-616, KZR-59177 and KZR-59240 in monkeys

Given the apparent difference in metabolic stability seen *in vitro*, we next studied the pharmacokinetics (PK) of KZR-616, KZR-59177 and KZR-59240 in cynomolgus monkeys following single subcutaneous (SC) administration of 3 mg/kg. As shown in Table 2, total exposures (area under the curve from zero to infinity, AUC_{inf}) were highest with KZR-59240, followed by KZR-616 and KZR-59177. The diol derivatives were

Downloaded from dmd.aspetjournals.org at ASPET Journals on April 16, 2024

DMD Fast Forward. Published on July 7, 2021 as DOI: 10.1124/dmd.120.000307
This article has not been copyedited and formatted. The final version may differ from this version.

determined to be the major metabolites for each compound and the AUC ratios (diol: parent) were 3.40 ± 0.81, 3.35 ± 1.20 and 0.78 ± 0.46 for KZR-616, KZR-59177, and KZR-59240, respectively. The PK of both parent and diol for each compound were consistent with the stability results in MLM in the absence of NADPH, in which the CYP enzymes were not activated. Interestingly, administration of KZR-59240, which was resistant to diol formation *in vitro*, resulted in a significant level of diol formation (AUC ratio of diol/parent: 0.78 ± 0.46) in monkeys.

Involvement of human mEH and sEH on KZR-616 epoxide hydrolysis KZR-616 is structurally related to carfilzomib, which is also metabolized to the inactive diol *in vivo* (Table 2). Since epoxide hydrolysis was identified to be the major metabolic pathway of KZR-616 *in vivo*, we assessed the contribution of mEH and sEH on diol formation from KZR-616 and carfilzomib using recombinant enzymes. Formation of the diol derivatives of KZR-616 (Figure 3A) and carfilzomib (Figure 3B) increased with an increase of mEH from 2 to 10 µg/mL, but no significant diol derivatives were detected for either compound in the presence of recombinant sEH up to 200 µg/mL. Epoxide hydrolysis of KZR-616 was also investigated in human and monkey liver microsomes (containing mEH) and hepatic cytosols (containing sEH). Probe substrates *cis*-SO (50 µM) and *trans*-SO (50 µM) were used as controls for mEH and sEH activity, respectively (Supplemental Figure 2). Similar to findings using recombinant enzymes, diol formation increased with increasing liver microsomal concentration, but minimal diol formation was seen in incubations with hepatic cytosols (Figure 3C and 3D). Taken together, these data indicate that the epoxide hydrolysis of KZR-616 and carfilzomib is mediated predominantly by mEH and that sEH plays little to no role in the metabolism of these compounds.

Downloaded from dmd.aspetjournals.org at ASPET Journals on April 16, 2024

DMD Fast Forward. Published on July 7, 2021 as DOI: 10.1124/dmd.120.000307
This article has not been copyedited and formatted. The final version may differ from this version.

KZR-616 metabolism in human hepatocytes and plasmas

Next, we quantitatively evaluated the disappearance of KZR-616 and the formation of KZR-59587 and additional metabolites in human hepatocytes. The metabolites identified following exposure of KZR-616 for 2 hr is shown in Figure 4-3a. Direct epoxide hydrolysis was the major pathway of KZR-616 in this system. Only trace levels of additional metabolites, including from demethylation and oxidation, and the combination of oxidation and epoxide hydrolysis were detected. The MS/MS spectrum of each metabolite were displayed in figure 4-1.

We used 1-ABT (a pan-CYP inhibitor), NSPA (an inhibitor of mEH) and TPPU (an inhibitor of sEH) to evaluate these metabolic pathways. There was no difference in the rate of clearance of KZR-616 upon CYP inhibition (Figure 4-2) with intrinsic clearance values of 16.5 ± 0.306 and 18.6 ± 0.400 μL/min/10^6 cells in the presence and absence of 1-ABT, respectively. Recovery of KZR-616 and diol was around 100% over the 60-minute time course. Similarly, elimination of KZR-616 and formation of diol was not affected by concentrations of TPPU up to 200 μM. In contrast, NSPA affected both the loss of parent and formation of diol, indicating that mEH plays the primary role in the metabolism of KZR-616 in human hepatocytes.

The metabolites identified in human plasma from 4 patients (0-8 h post dose) receiving a 75 mg dose of KZR-616 are shown in Figure 4-3b. KZR-59587 (diol) was identified to be the major metabolite. KZR-59587 and its parent KZR-616 were quantified as peak area percentage of total peak area of KZR-616 and all observed metabolites were 33.8 and 61.2; 45.8 and 49.0; 47.9 and 46.5; 43.8 and 51.8, respectively for the 4 patients (Table 4). Other metabolites including the isomer of KZR-59587, oxidation, hydrolysis and

Downloaded from dmd.aspetjournals.org at ASPET Journals on April 16, 2024

DMD Fast Forward. Published on July 7, 2021 as DOI: 10.1124/dmd.120.000307
This article has not been copyedited and formatted. The final version may differ from this version.

dehydrogenation, and double oxidation of KZR-616 were all less than 1% of total peak area of KZR-616 and metabolites.

Kinetics of KZR-616 epoxide hydrolysis Next, we determined the reaction kinetics of diol formation using human recombinant mEH, HLMs, human hepatocytes across a wide range of KZR-616 concentrations (0 –1000 µM). Optimized enzyme concentrations and incubation times were applied to ensure that initial mEH-mediated hydrolysis was in the linear product formation range for accurate estimation (Figure 6). Inhibition of epoxide hydrolysis of KZR-616 and *cis*-SO by NSPA was evaluated in parallel. NSPA inhibited mEH-mediated hydrolysis for KZR-616 with mean IC_{50} values ranging from 0.409 to 0.826 µM across the different test systems (Figure 7). From these experiments, we were able to obtain kinetic constants (K_m), maximum velocities (V_{max}) and efficiency (V_{max}/K_m) of KZR-616 epoxide hydrolysis (Table 3). As expected, the greatest metabolic efficiency was observed with recombinant mEH. Metabolic efficiencies of female/male human and monkey liver microsome were 0.33-0.45% and 4.5-4.6% of recombinant mEH, respectively, suggesting that mEH levels are lower in HLM vs. MLM.

Finally, we sought to determine if KZR-616 could inhibit EH activity in recombinant enzymes, LM or intact cells. Epoxide hydrolysis of *cis*-SO by mEH and epoxide hydrolysis of *trans*-SO by sEH were unaffected by the presence of KZR-616 at concentrations up to 100 µM (Figure 8).

Downloaded from dmd.aspetjournals.org at ASPET Journals on April 16, 2024

DMD Fast Forward. Published on July 7, 2021 as DOI: 10.1124/dmd.120.000307
This article has not been copyedited and formatted. The final version may differ from this version.

Discussion

Targeted covalent inhibitors provide several advantages over conventional reversible inhibitors, including increased efficacy and selectivity (Leung et al., 2017). Peptide epoxyketone-based proteasome inhibitors, such as carfilzomib and oprozomib, can induce prolonged pharmacodynamic effects despite rapid clearance and short systemic exposure *in vivo* due in part to covalent modification of proteasome active sites (Yang et al., 2011; Wang et al., 2013). These compounds are primarily metabolized to the in active diol via epoxide hydrolysis, which renders the molecule inactive. Given this nontraditional metabolic pathway, there are currently no well-characterized *in vitro* test systems to study the metabolic properties of this class of compounds. KZR-616 is a novel peptide epoxyketone that was designed to selectively bind the immunoproteasome active sites, LMP7 and LMP2, and is currently being evaluated in Phase 2 clinical trials in autoimmune disorders (Johnson et al., 2018). We studied KZR-616 and its analogs in multiple *in vitro* test systems ranging from recombinant enzymes to live cell incubation and compared those data to clearance values following administration to non-human primates in an effort to determine optimal *in vitro* test systems for future medicinal chemistry campaigns.

In this work, we attempted to develop ADME assays that can be used for screening for irreversible covalent proteases inhibitors. During the drug discovery stage, a challenge we encountered was to find an optimum *in vitro* test system that can correlate with *in vivo* PK results. Three tool compounds (KZR-616, KZR-59177 and KZR-59240) were used to study their metabolic stabilities in human and monkey liver microsomes (LM) in the presence and absence of NADPH. We found that the CL_{int} of these compounds was

Downloaded from dmd.aspetjournals.org at ASPET Journals on April 16, 2024

DMD Fast Forward. Published on July 7, 2021 as DOI: 10.1124/dmd.120.000307
This article has not been copyedited and formatted. The final version may differ from this version.

driven by CYP plus EH in the presence of NADPH, but only by EH in the absence of NADPH and that CYP3A4/5 was the major isoform of CYP driving metabolism in the presence of NADPH in LM. However, PK data revealed that their diol derivatives were the predominant metabolites, indicating that mEH play a major role in the *in vivo* and that CYP mediated metabolism is not involved. This implies that the *in vitro* LM test system doesn't generate a correlated or indicative metabolic result.

By using monkey hepatocytes, we found that diol derivatives were the major metabolites for these compounds, indicating that the mEH play a major role in the hepatocyte system and correlating with PK results. The clinical candidate KZR-616 was further investigated in human hepatocytes. The metabolism profiling of KZR-616 in human hepatocytes indicated that the diol KZR-59587 generated from mEH metabolic pathway was the major metabolite of KZR-616 and only trace levels of other metabolites from oxidation and dehydrogenation pathways. Using the inhibitors of CYP and EHs to study KZR-616 metabolism in human hepatocytes also concluded that mEH mediated metabolic is the major pathway. Similar to the monkey system, metabolism profiling of human plasma samples from patients receiving KZR-616 revealed that the diol KZR-59587 as the major metabolite. All other metabolites were all less than 1% of total of the parent and the observe metabolites. Therefore, the monkey system, both *in vitro* and *in vivo*, were predictive of the ADME properties of KZR-616 in humans.

Liver microsomes are a widely used *in vitro* test system for high throughput ADME screening in lead compound discovery programs. However, concerns related to the correlation with *in vivo* study results and over-estimation of CYP activity have recently been reported (Tinglea et al., 2005; Brown et al., 2007). In the presence of NADPH, a

Downloaded from dmd.aspetjournals.org at ASPET Journals on April 16, 2024

necessary co-factor for CYP activity in LM preparations, KZR-616 and its analogs were rapidly cleared, but the recovery of parent and diol was poor (~50% in 1h), indicating that there were other metabolic pathways involved. However, in the absence of NADPH, the stability with varying degrees were observed across 79 related compounds. Diol products were also the major metabolite found following administration of KZR-616 and two other structurally related compounds to monkeys. The PK exposures measured *in vivo* for these compounds correlated well with the observed stability in LM incubations in the absence of NADPH. Interestingly, for KZR-59240, which was stable in LM incubations and showed minimal diol formation, significant formation of the diol metabolite (KZR-59433) was measured *in vivo*. The discrepancy between the metabolite detection from standard LM cultures in the absence of NADPH and *in vivo* pharmacokinetic studies indicates that EH enzymatic activities might be lost during microsome preparation or suppressed by other enzymes in LM test systems.

To overcome the major deficiency of using LM to study peptide epoxyketone metabolism, we used cryopreserved human hepatocytes as an *in vitro* test system. Intact hepatocytes contain both Phase I and II metabolism enzymes and likely provide a more comprehensive system to correlate *in vitro* test results with *in vivo* PK (McGinnity et al., 2004; Newman JW et al., 2005; Brown et al., 2007). Similar to what was observed in PK studies, the predominant metabolite of KZR-616 found following incubations with intact hepatocytes was the diol. As demonstrated using enzyme-specific probe substrates, hepatocytes contain both sEH and mEH, and we used isoform-specific inhibitors to phenotype KZR-616 metabolism. Diol formation was blocked by the mEH inhibitor, NSPA, but neither TPPU (a sEH inhibitor), nor ABT-1 (a pan-CYP inhibitor) had an

Downloaded from dmd.aspetjournals.org at ASPET Journals on April 16, 2024

impact on diol formation or loss of parent compound. Thus, using human hepatocytes we were able to match the metabolite profile seen *in vivo* as well as determine the specific enzyme responsible for diol formation from KZR-616.

Epoxide hydrolases are a ubiquitously expressed family of enzymes found in mammals (Morisseau, 2013; Wazers et al., 1990; Gautheron, et al., 2021; Enayetallah, et al., 2006) and are the primary pathway for the detoxification of compounds containing an epoxide residue (Decker et al., 2009). There are 2 major isoforms, mEH, encoded by the EPHX1 gene and localized predominantly in the endoplasmic reticulum, and sEH, encoded by the EPHX2 gene and confined mainly to cytoplasm (Larsson et al., 1995). Both are highly expressed in mammalian hepatocytes (Gill and Hammock, 1980; Coller et al., 2001). Using human hepatocytes ells, we determined that mEH is the primary enzyme mediating metabolism of KZR-616 and its analogs. Enzymatic kinetic constants for KZR-616 epoxide hydrolysis were determined using recombinant enzymes, LM, and in intact cells. These studies revealed that the EH-mediated metabolic efficiency of LM was <5% of the recombinant enzyme and that hepatocytes are a more efficient cell-based system for epoxide hydrolysis. Given that mEH also mediates metabolism of carfilzomib and oprozomib, this represents a common pathway for metabolism of this class of compound. It is noteworthy that unlike KZR-616, both carfilzomib and oprozomib show peptidase hydrolysis as an additional metabolic pathway *in vivo* (Wang et al., 2013; Wang et al., 2017). It is also interesting that *in vitro* plasma stability studies of CFZ and KZR-616 in monkey (data not shown) at 37°C for 6 h did not produce any peptide cleavage metabolites, and the epoxide hydrolysis metabolites (diol) were below LOQ for

Downloaded from dmd.aspetjournals.org at ASPET Journals on April 16, 2024

both compounds indicating lacking both peptidase and mEH in commercial monkey plasmas.

In conclusion, through a thorough analysis of *in vitro* test systems and analysis of pharmacokinetic data, the predominant metabolic pathway of KZR-616 was determined to be epoxide hydrolysis via the action of mEH. These data suggest that the PK of KZR-616 is unlikely to be affected by co-administration of CYP and sEH inhibitors/inducers and that KZR-616 is unlikely to alter epoxide hydrolysis of other mEH and sEH substrate drugs. Given the widespread tissue distribution and the efficiency of KZR-616 metabolism measured with recombinant enzyme, it would be difficult to saturate this process *in vivo*. This suggests a low risk for altered exposure to KZR-616 upon co-administration of known or suspected mEH inhibitors.

The work presented here describes a series of *in vitro* and cell-based enzymatic metabolism and kinetic investigations for peptide epoxyketone analogs. Despite some described limitations, hepatocytes served as a good *in vitro* test system to assess the metabolic profiles of KZR-616 and other peptide epoxyketones and could be useful in assessing novel covalent proteasome inhibitors during lead compound optimization.

Downloaded from dmd.aspetjournals.org at ASPET Journals on April 16, 2024

Acknowledgement

We thank Celia Economides, Kiruthi Palaniswamy, Michelle Greenman, and Mark Shiller from Kezar Life Sciences for reviewing the manuscript and helpful suggestions.

Authorship Contributions

Participated in research design: Fang, Kirk, Wang.

Conducted experiments: Fang, Anderl, Johnson, McMinn, Muchamuel, Wang.

Contributed new reagent or analytic tools: Morisseau, Hammock.

Performed data analysis: Fang, Wang.

Wrote or contributed to the writing of the manuscript: Fang, Kirk, Wang, Morisseau, Hammock.

Downloaded from dmd.aspetjournals.org at ASPET Journals on April 16, 2024

DMD Fast Forward. Published on July 7, 2021 as DOI: 10.1124/dmd.120.000307
This article has not been copyedited and formatted. The final version may differ from this version.

References

Basler M and Groettrup M (2012). Immunoproteasome-specific inhibitors and their application. *Methods Mol Biol* 832:391-401.

Basler M, Mundt S, Bitzer A, Schmidt C, Groettrup M (2015) The immunoproteasome: a novel drug target for autoimmune diseases. *Clin Exp Rheumatol* 33: S74-79.

Bross PF1, Kane R, Farrell AT, Abraham S, Benson K, Brower ME, Bradley S, Gobburu JV, Goheer A, Lee SL, Leighton J, Liang CY, Lostritto RT, McGuinn WD, Morse DE, Rahman A, Rosario LA, Verbois SL, Williams G, Wang YC, Pazdur R (2004) Approval summary for bortezomib for injection in the treatment of multiple myeloma. *Clin Cancer Research* 10: 3954-3964.

Brown HS, Griffin M and Houston JB (2007) Evaluation of Cryopreserved Human Hepatocytes as an Alternative in Vitro System to Microsomes for the Prediction of Metabolic Clearance. *Drug Metab and Dispos* 35: 293-301.

Catharina Larsson, Irene White, Charlotte Johansson, Annika Stark & Johan Meijer (1995) Localization of the human soluble epoxide hydrolase gene (EPHX2) to chromosomal region 8p21-P12. *Human Genetics* 95:356–358.

Coller JK1, Fritz P, Zanger UM, Siegle I, Eichelbaum M, Kroemer HK, Mürdter TE. (2001) Distribution of microsomal epoxide hydrolase in humans: an immunohistochemical study in normal tissues, and benign and malignant tumors. *Histochem J* 33:329-336.

Deborah A. (2012) Ferrington ad Sale S. Gregerson Immunoproteasomes: Structure, Function, and Antigen presentation. *Prog Mol Biol Transl Sci* 109: 75-112.

Downloaded from dmd.aspetjournals.org at ASPET Journals on April 16, 2024

Decker M, Arand M, Cronin A (2009) Mammalian epoxide hydrolases in xenobiotic metabolism and signalling. *Arch Toxicol* 83:297-318.

Demo SD, Kirk CJ, Aujay MA, Buchholz TJ, Dajee M,Ho MN, Jiang J, Laidig GJ, Lewis ER, Parlati F, Shenk KD, Smyth MS, Sun M, Vallone MK, Woo T, Molineaux CJ and Bennett MK (2007) Antitumor Activity of PR-171, a Novel Irreversible Inhibitor of the Proteasome. *Cancer Res* 67: (13).

Egerer T, Martinez-Gamboa L, Dankof A,1Bruno Stuhlmuller B, Dorner T, Krenn V, Egerer K, Rudolph PE, Burmester GR and Feist E (2006) Tissue-Specific Up-Regulation of the Proteasome Subunit β5i (LMP7) in Sjo¨gren's Syndrome. *Arthritis & Rheumatism* 54:1501-1508.

Enayetallah, A E, French R, and Grant D F (2006) Distribution of soluble hydrolase, cytochrome P450, 2C6, 2C9, and 2J2 in human malignant neoplasms. *J. Mol. Hist* 37 (3-4):133-41.

Gautheron J, Jeru I (2021) The multifaceted role of epoxide hydrolases in human health. *Int. J. Mol. Sci.* 22 (1):13-30.

Gentile M, Offidani M, Vigna E, Corvatta L, Recchia AG, Morabito L, Morabito F, Gentili S (2015) Ixazomib for the treatment of multiple myeloma. *Expert Opin Investig Drugs* 24 (9):1287-98.

Groettrup M, Kirk CJ, Basler M (2010) Proteasomes in immune cells: more than peptide producers? *Nat Rev Immunol* 10(1):73-78.

Gill SS and Hammock BD (1980) Distribution and properties of a mammalian soluble epoxide hydrase. *Biochem Pharmacol* 29:389-395.

Downloaded from dmd.aspetjournals.org at ASPET Journals on April 16, 2024

Harshbarger W, Miller C, Diedrich C, and Sacchettini J (2015) Crystal Structure of the Human 20S Proteasome in Complex with Carfilzomib. *Structure* 23: 418-424.

Hartsfield J.K, Sutcliffe M.J, Everett E.T., Hassett C, Omiecinskif f C.J. and. Saaric J.A (1998) Assignment of microsomal epoxide hydrolase (EPHX1) to human chromosome 1q42.1 by in situ hybridization (EPHX1) to human chromosome. *Cytogenet Cell Genet* 83:44–45.

Herndon TM, Deisseroth A, Kaminskas E, Kane RC, Koti KM, Rothmann MD, Habtemariam B, Bullock J, Bray JD, Hawes J (2013) U.S. Food and Drug Administration Approval: Carfilzomib for the Treatment of Multiple. *Clin Cancer Res* 19:4559–4563.

Johnson HWB, Lowe E, Anderl JL, Fan A, Muchamuel T, Bowers S, Moebius DC, Kirk C, and McMinn DL (2018) Required Immunoproteasome Subunit Inhibition Profile for Anti-Inflammatory Efficacy and Clinical Candidate KZR-616 ((2S,3R)-N-((S)-3-(Cyclopent-1-en-1-yl)-1-((R)-2-methyloxiran-2-yl)-1oxopropan-2-yl)-3-hydroxy-3-(4-methoxyphenyl)-2-((S)-2-(2morpholinoacetamido)propanamido)propenamide). *J. Med. Chem* 61:11127−11143.

Institute of Laboratory Animal Resources (1996) Guide for the Care and Use of Laboratory Animals. 7th ed, Institute of Laboratory Animal Resources, Commission on Life Sciences, National Research Council, Washington DC.

Kapur SA, Anderl JL, Kraus M, Parlati F, Shenk KD, Lee SJ, Muchamuel T, Bennett MK, Driessen C3, Ball AJ , and Kirk CJ (2011) Non-proteasomal Targets of the Proteasome Inhibitors Bortezomib and Carfilzomib: a Link to Clinical. *Clin Cancer Res 17(9):* 2734-2743.

Downloaded from dmd.aspetjournals.org at ASPET Journals on April 16, 2024

Kerr BM, Rettie AE, Eddy AC, Loiseau P, Guyot M, Wilensky AJ, Levy RH (1989) Inhibition of human liver microsomal epoxide hydrolase by valproate and valpromide: in vitro/in vivo correlation. *Clin Pharmacol Ther* 46 (1): 82-93.

Kisselev AF and Goldberg AL (2001) Proteasome inhibitors: from research tool to drug candidates. *Chem Biol* 8: 739-758017: 2559.

Kisselev A F, Linden W A, Overkleeft H S (2012) Proteasome inhibitors: an expanding army attacking a unique target *Chem Biol*:19 (1): 99-115.

Kitteringham NR, Davis C, Howard N, Pirmohamed M and Park BK (1996) Interindividual and Interspecies Variation in Hepatic Microsomal Epoxide Hydrolase Activity: Studies with cis-Stilbene Oxide, Carbamazepine 10, 11 -Epoxide and Naphthalene. *J Pharmacol Exp Ther* 278: 1018-1027.

Krishna P, Elliott JL (2005) Non-neuronal induction of immunoproteasome subunits in an ALS model: Possible mediation by cytokines. *J Expneurol* 196: 441-451.

Kunh DJ, Chen Q, Voorhees PM, Strader JS, Shenk KD, Sun CM, Demo SD, Bennett MK, van Leeuwen FW, Chanan-Khan AA, and Orlowski RZ (2007) Potent activity of Carfilzomib, a novel, irreversible inhibitor of the ubiquitin-proteasome pathway, against preclinical models of multiple myeloma. *Blood* 110: 3281-3290.

Larsson C, White I, Johansson C, Stark A, Meijer J (1995) Localization of the human soluble epoxide hydrolase gene (EPHX2) to chromosomal region 8p21-p12 *Human Genetics*:95: 356-358.

Leung L, Yang X, Strelevitz TJ, Montgomery J, Brown MF, Zientek MA, Banfield C, Gilbert AM, Thorarensen A and Dowty ME (2017) Clearance Prediction of Targeted

Downloaded from dmd.aspetjournals.org at ASPET Journals on April 16, 2024

Covalent Inhibitors by In Vitro-In Vivo Extrapolation of Hepatic and Extrahepatic Clearance Mechanisms *Drug Metab and Dispos* 45:1-7.

McGinnity DF, Soars MG, Urbanowicz RA and Riley RJ (2004) Evaluation of fresh and cryopreserved hepatocytes as in vitro drug metabolism tools for the prediction of metabolic clearances. *Drug Metab and Dispos* 32: 1247-1253.

Miller Z, Ao L, Kim KB, Lee W (2013). Inhibitors of the immunoproteasome: Current status and future directions. *Curr Pharm Des* 19: 4140-4151.

Montellano PR (2018) 1-Aminobenzotriazole: A Mechanism-Based Cytochrome P450 Inhibitor and Probe of Cytochrome P450. *Biology Med Chem* 8: 038.

Morisseau C, Newman JW, Wheelock CE, Iii TH, Morin D, Buckpitt AR, Hammock BD (2008) Development of metabolically stable inhibitors of Mammalian microsomal epoxide hydrolase. *Chem Res Toxicol* 21(4):951-7.

Morisseau C (2013) Role of epoxide hydrolases in lipid metabolism. *Biochimie* 95(1): 91–95.

Muchamuel T, Anderl J, Fan RA, Johnson HW.B., Kirk CJ, Eric Lowe E (2017) KZR-616, a selective inhibitor of the immunoproteasome, Blocks the disease progression in multiple models of systemic lupus Erythematosus (SLE). *ACR/ARHP Annual Meeting 2.*

Newman JW, Morisseau C, Harris TR, and Hammock BD (2003) The soluble epoxide hydrolase encoded by EPXH2 is a bifunctional enzyme with novel lipid phosphate phosphatase activity. *PNAS* 100: 1558-1563.

Newman JW, Morisseau C, Hammock BD (2005) Epoxide hydrolases: their roles and interactions with lipid metabolism. *Prog. Lipid Res* 44:1–51.

Downloaded from dmd.aspetjournals.org at ASPET Journals on April 16, 2024

Offidani M, Corvatta L, Caraffa P, Gentili S, Maracci L, Leoni P (2014) An evidence-based review of ixazomib citrate and its potential in the treatment of newly diagnosed multiple myeloma. *Onco Targets Ther* 7:1793-800.

Puttaparthi K, and Elliott JL (2005) Non-neuronal induction of immunoproteasome subunits in an ALS model: possible mediation by cytokines *Exp Neurol* 196 (2): 444-51.

Teicher, B.A Tomaszewski J. E. (2015) Proteasome inhibitors. *Biochemical Pharmacology* 96: 1-9.

Tinglea M.D. and Helsbyb N.A. (2005) Can in vitro drug metabolism studies with human tissue replace in vivo animal studies? *Environmental Toxi and Pharmac* 21: 184-190.

Wang Z, Yang J, Kirk C, Fang Y, Alsina M, Badros A, Papadopoulos K, Wong W, Woo T, Bomba D, Li J and Infante JR (2013) Clinical Pharmacokinetics, Metabolism, and Drug-Drug Interaction of Carfilzomib. *Drug Metab and Dispos* 41:230-237.

Wazers J De, Cugnenc P H, Yang C S, Leroux J P, and Beaune P H (1990) Cytochrome P450 isoenzymes, epoxide hydrolase and glutathione transferases in rat and human hepatic and extrahepatic tissues. *J. Pharmacology and Experimental Therapeutics* 253 (1):387-394.

Václavíková RV, Hughes DJ, Souček P. (2015) Microsomal Epoxide Hydrolase 1 (EPHX1): Gene, Structure, Function, and Role in Human Disease. *Gene* 571: 1–8.

Wang Z, Fang Y, Teague J, Wong H, Morisseau C, Hammock BD, Rock DA and Wang Z (2017) In Vitro Metabolism of Oprozomib, an Oral Proteasome Inhibitor: Role of Epoxide Hydrolases and Cytochrome P450s. *Drug Metab and Dispos* 45 :712-720.

Downloaded from dmd.aspetjournals.org at ASPET Journals on April 16, 2024

Yang J, Wang Z, Fang Y, Jiang J, Zhao F, Wong H, Bennett MK, Molineaux CJ and Kirk CJ (2011) Pharmacokinetics, Pharmacodynamics, Metabolism, Distribution, and Excretion of Carfilzomib in Rat. *Drug Metab and Dispos* 39(10): 1873-1882.

Zhou HJ, Aujay MA, Bennett MK, Dajee M, Demo SD, Fang Y, Ho MN, Jiang J, Kirk CJ, Laidig GJ, Lewis ER, Lu Y, Muchamuel T, Parlati F, Ring E, Shenk KD, Shields J, Shwonek PJ, Stanton T, Sun CM, Sylvain C, Woo TM, Yang J (2009) Design and synthesis of an orally bioavailable and selective peptide epoxyketone proteasome inhibitor (PR-047). *J Med Chem*. 52:3028-38.

Reference patents:

McMinn, D.; Johnson, H.; Moebius, D. C. Dipeptide and tripeptide epoxy ketone protease inhibitors, Patent Appl. US9657057B2.

McMinn, D.; Johnson, H.; Bowers, S.; Moebius, D. C. Tripeptide epoxy ketone protease inhibitors 3.1 , Patent Appl. US10647744B2

Footnote

The work was supported by Kezar Life Sciences

Conflicts of Interest: The authors declare that They have no competing interests

Downloaded from dmd.aspetjournals.org at ASPET Journals on April 16, 2024

DMD Fast Forward. Published on July 7, 2021 as DOI: 10.1124/dmd.120.000307
This article has not been copyedited and formatted. The final version may differ from this version.

Legends for Figures

Figure 1: Chemical structures of KZR-616, KZR-59177, KZR-59240, their diol derivatives, carfilzomib, and oprozomib.

Figure 2: A) Metabolism of KZR-616 and analogs in human and monkey liver microsomes in the absence of NADPH Percentages of detected residual KZR-616, KZR-59177, KZR-59240 and a total of 79 analogs in HLM (0.5 mg/mL) or MLM (0.25 mg/mL) in the absence of NADPH. Initial concentrations of KZR-616 and analogs were 1 µM. Residual concentrations of KZR-616 and analogs were quantified using LC-MS/MS assays. Data are presented as mean ± SD from triplicate incubations.

B) **Metabolism of KZR-616 and analogs in monkey hepatocytes**. Percentage of KZR-616, KZR-59177 and KZR-59240 remaining, and their diol formation from initial parents in monkey hepatocytes (0.25 x10^6 cells/mL) after 40 min incubation. The initial concentration of parents was 1 µM. Concentrations of parents and their diols were quantified using LC-MS/MS analysis. Data are presented as mean ± SD from duplicate incubations.

Figure 3: Epoxide hydrolysis of KZR-616 and carfilzomib in recombinant mEH and sEH; epoxide hydrolysis of KZR-616 in HLM, MLM, and human and monkey cytosol A) Epoxide hydrolysis of KZR-616 in recombinant human mEH (2-10 µg/mL) and sEH (20-100 µg/mL). B) Epoxide hydrolysis of carfilzomib in recombinant human mEH (2-10 µg/mL) and sEH (20-200 µg/mL). C) Epoxide hydrolysis of KZR-616 in HLM (0.25-1 mg/mL) and human cytosol (0.4-1 mg/mL). D) Epoxide hydrolysis of KZR-616 in MLM (0.2-1 mg/mL) and monkey cytosol (0.1-1 mg/mL). The

Downloaded from dmd.aspetjournals.org at ASPET Journals on April 16, 2024

DMD Fast Forward. Published on July 7, 2021 as DOI: 10.1124/dmd.120.000307
This article has not been copyedited and formatted. The final version may differ from this version.

concentrations of KZR-616, carfilzomib and their diols were quantified using LC-MS/MS assays. Data are presented as mean ± SD from triplicate incubations.

Figure 4-1: The MS/MS spectrum of identified metabolites

The metabolites identified from the 2 hour incubations in human hepatocytes (2.0 x10^6 cells/mL)

4-2) KZR-616 metabolism in human hepatocytes and effect of 1-ABT, NSPA and TPPU A) Percentage of KZR-616 remaining in human hepatocytes in the presence or absence of 1-ABT. B) Formation of diol KZR-59587 in human hepatocytes in the presence or absence of 1-ABT. C) Percentage of KZR-616 remaining in human hepatocytes in the presence or absence of NSPA and TPPU. D) Formation of diol KZR-59587 in human hepatocytes in the presence or absence of NSPA and TPPU. The concentration of cryopreserved human hepatocytes in incubations was 0.5 x10^6 cells/mL. The initial concentration of KZR-616 was 1 µM. The concentrations of inhibitors were 0.5 mM, 10 µM and 200 µM for 1-ABT, NSPA and TPPU, respectively. Concentrations of KZR-616 and KZR-59587 were quantified using LC-MS/MS analysis. Data are presented as mean ± SD from duplicate incubations.

4-3) The metabolic pathways of KZR-616 in human hepatocytes and plasmas.

4-3a: The metabolite identification following exposure of KZR-616 (10 µM) in pooled cryopreserved human hepatocytes (2x10^6 cells/mL) for 2 h.

4-3b: The metabolite identification in human plasma from 4 patients (0-8 h post dose) receiving a 75 mg dose of KZR-616.

Downloaded from dmd.aspetjournals.org at ASPET Journals on April 16, 2024

DMD Fast Forward. Published on July 7, 2021 as DOI: 10.1124/dmd.120.000307
This article has not been copyedited and formatted. The final version may differ from this version.

Figure 5: Kinetics of epoxide hydrolysis of KZR-616 in HLM, MLM, recombinant human mEH and human hepatocytes A) Kinetics of diol KZR-59587 formation in male and female HLM, MLM and recombinant human mEH were performed at 37°C for 30 min. B) Kinetics of the formation of KZR-59587 in human hepatocytes cells at 37°C for 30 min. The K_m and V_{max} values were estimated by fitting the curve to the Michaelis-Menten equation. Data represent mean ± SD from duplicate incubations.

Figure 6: Inhibition of epoxide hydrolysis of KZR-616 in HLM, MLM, human hepatocytes and recombinant human mEH by NSPA A) Inhibition of mEH activity by NSPA in male and female HLM. B) Inhibition of mEH activity by NSPA in male and female MLM. C) Inhibition of mEH activity by NSPA in human hepatocytes. D) Inhibition of mEH activity by NSPA in recombinant human mEH. The IC_{50} values were estimated using nonlinear regression data analysis. Data are presented as mean ± SD from duplicate incubations.

Figure 7: Inhibition of epoxide hydrolysis of probe substrates *cis*-SO and *trans*-SO by KZR-616 A) Scheme of *cis*-SO metabolism and inhibition of *cis*-SO hydrolysis by KZR-616. B) Scheme of *trans*-SO metabolism and inhibition of *trans*-SO hydrolysis by KZR-616. The diol derivatives of *cis*-SO and *trans*-SO (R, R-Hydrobenzoin and Meso-Hydrobenzoin) were quantified by using LC-UV methods.

Downloaded from dmd.aspetjournals.org at ASPET Journals on April 16, 2024

DMD Fast Forward. Published on July 7, 2021 as DOI: 10.1124/dmd.120.000307
This article has not been copyedited and formatted. The final version may differ from this version.

Table 1. In vitro metabolic stability of KZR-616 and analogs in HLM and MLM in the presence or absence of NADPH.

Predicted $T_{1/2}$ and Cl_{int} were obtained from in vitro assays. Data are presented as mean ± SD (n=3). The concentration of test compound in the assays was 1 µM.

ID	KZR-616				KZR-059177				KZR-059240			
Species	HLM		MLM		HLM		MLM		HLM		MLM	
(NADPH)	(-)	(+)	(-)	(+)	(-)	(+)	(-)	(+)	(-)	(+)	(-)	(+)
$T_{1/2}$ (min)	194 ± 14.0	76.0 ± 3.7	97.1 ± 12.6	16.0 ± 0.433	39.1 ± 1.07	16.2 ± 0.793	24.2 ± .719	12.4 ± 2.78	NA	45.6± 4.61	NA	18.1± 2.16
Cl_{int} (µl/min/mg)	14.3 ± 1.01	36.5 ± 1.80	28.6±3.67	173 ±.4.62	70.9 ± 1.97	172 ± 8.51	2860 ± 84.5	5717 ± 1274	NA	51.2± 0.621	NA	154 ± 18.4
LM binding (%)	12.3		7.40		NA		NA		20.4		21.3	

NA: Not applicable (No value was obtained).

LM binding (%) of test compound was conducted using ultracentrifugation

Downloaded from dmd.aspetjournals.org at ASPET Journals on April 16, 2024

DMD Fast Forward. Published on July 7, 2021 as DOI: 10.1124/dmd.120.000307
This article has not been copyedited and formatted. The final version may differ from this version.

Table 2. PK parameters of KZR-616 and analogs after a single SC dose at 3 mg/kg in monkeys

ID	KZR-59177	KZR-616	KZR-59240
$T_{1/2}$ (hr)	1.44 ± 0.420	1.05 ± 0.130	0.980 ± 0.264
T_{max} (hr)	0.792 ± 0.417	0.333 ± 0.136	0.500 ± 0.334
C_{max} (ng/mL)	182 ± 31.5	441 ± 114	803 ± 260
AUC_{inf} (hr*ng/mL)	447± 57.3	740 ± 188	1412 ± 279
AUC Ratio (diol/parent)	3.35 ± 1.20	3.40 ± 0.808	0.777 ± 0.464
% Unbound fraction	NA	42.2	NA

Downloaded from dmd.aspetjournals.org at ASPET Journals on April 16, 2024

DMD Fast Forward. Published on July 7, 2021 as DOI: 10.1124/dmd.120.000307
This article has not been copyedited and formatted. The final version may differ from this version.

Table 3. Summary of kinetic parameters from Michaelis-Menten analysis of epoxide hydrolysis of KZR-616 (data represent mean ± SD; duplicate incubations; efficiency defined as Vmax/Km).

Epoxide hydrolysis	Kinetics of the formation of KZR-59587 from *in vitro* enzymatic assays		
	Km (μM)	Vmax (nmol/min/mg protein)	Vmax/Km (% of mEH)
[a]Recombinant mEH	2172 ± 341	555 ± 64.1	0.256 ± 0.029
Male HLM	987 ± 338	17.2 ± 3.48	0.017 ± 0.004 (6.82%)
Female HLM	1862 ± 1065	24.2 ± 9.81	0.013 ± 0.0045 (5.07%)
Male MLM	178 ± 25.9	31.1 ± 1.57	0.175 ± 0.009 (68.4%)
Female MLM	191 ± 27.1	34.1 ± 1.72	0.179 ± 0.009 (69.9%)
Epoxide hydrolysis	Kinetics of the formation of KZR-59587 from cell-based assays		
	Km (μM)	Vmax (picomoles/min/10^6 cells)	Vmax/Km (% of hepatocytes)
[b]Human hepatocytes	76.7 ± 20.1	4674 ± 325	60.9 ± 4.23

a: Recombinant mEH used as control value for comparing the percentage efficiency amongst enzymatic assays

b. Human hepatocytes used as control value for comparing the percentage efficiency amongst cell-based assays.

Downloaded from dmd.aspetjournals.org at ASPET Journals on April 16, 2024

DMD Fast Forward. Published on July 7, 2021 as DOI: 10.1124/dmd.120.000307
This article has not been copyedited and formatted. The final version may differ from this version.

Table 4. Summary of KZR-616 and proposed metabolites observed in human plasma

Component Label	Identification	Retention Time (min)	$[M+H]^+$ (m/z)	Component in Plasma as % of Total [a]XIC Area			
				Subject			
				110-004	112-021	113-002	116-012
KZR-616	Parent	22.0	587.3	61.2	49.0	46.5	51.8
KZR-59587	Epoxide hydrolysis	16.4	605.3	33.8	45.8	47.9	43.8
M605_2	Epoxide hydrolysis (isomer)	14.5	605.3	0.270	0.270	0.270	0.280
M603_1	Oxidation	11.0	603.3	0.080	0.100	0.060	0.060
M603_7	Oxidation	11.8	603.3	0.100	0.250	0.040	0.170
M603_8	Oxidation	13.3	603.3	0.150	0.190	0.150	0.190
M603_2	Oxidation	15.0	603.3	0.080	0.020	0.080	0.060
M603_3	Oxidation	17.5	603.3	0.140	0.110	0.150	0.100
M603-4	Hydrolysis + dehydrogenation	20.2	603.3	0.280	0.420	0.290	0.240
M603_5	Hydrolysis + dehydrogenation	20.4	603.3	0.260	0.260	0.280	0.240
M603_6	Oxidation	22.8	603.3	0.390	0.340	0.410	0.330
M601	Oxidation + dehydrogenation	14.4	601.3	0.890	0.870	0.800	0.910
M619_1	Double Oxidation	9.71	619.3	0.280	0.280	0.160	0.190
M619_2	Double Oxidation	19.1	619.3	0.120	0.170	0.030	0.020

a: XIC = extracted-ion chromatogram in LC-MS analysis

Downloaded from dmd.aspetjournals.org at ASPET Journals on April 16, 2024

DMD Fast Forward. Published on July 7, 2021 as DOI: 10.1124/dmd.120.000307
This article has not been copyedited and formatted. The final version may differ from this version.

Figure 1

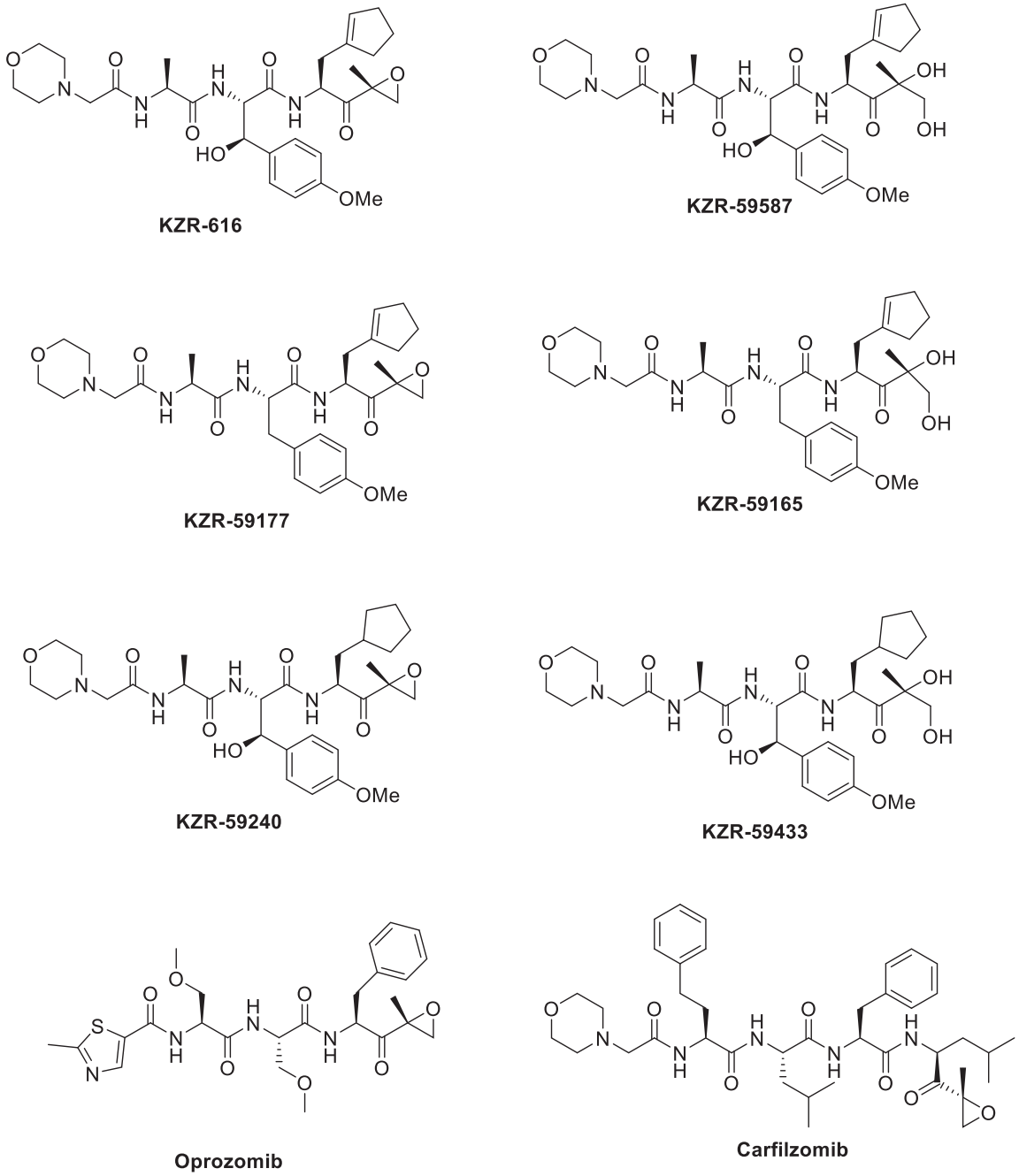

Downloaded from dmd.aspetjournals.org at ASPET Journals on April 16, 2024

DMD Fast Forward. Published on July 7, 2021 as DOI: 10.1124/dmd.120.000307
This article has not been copyedited and formatted. The final version may differ from this version.

Figure 2

A.

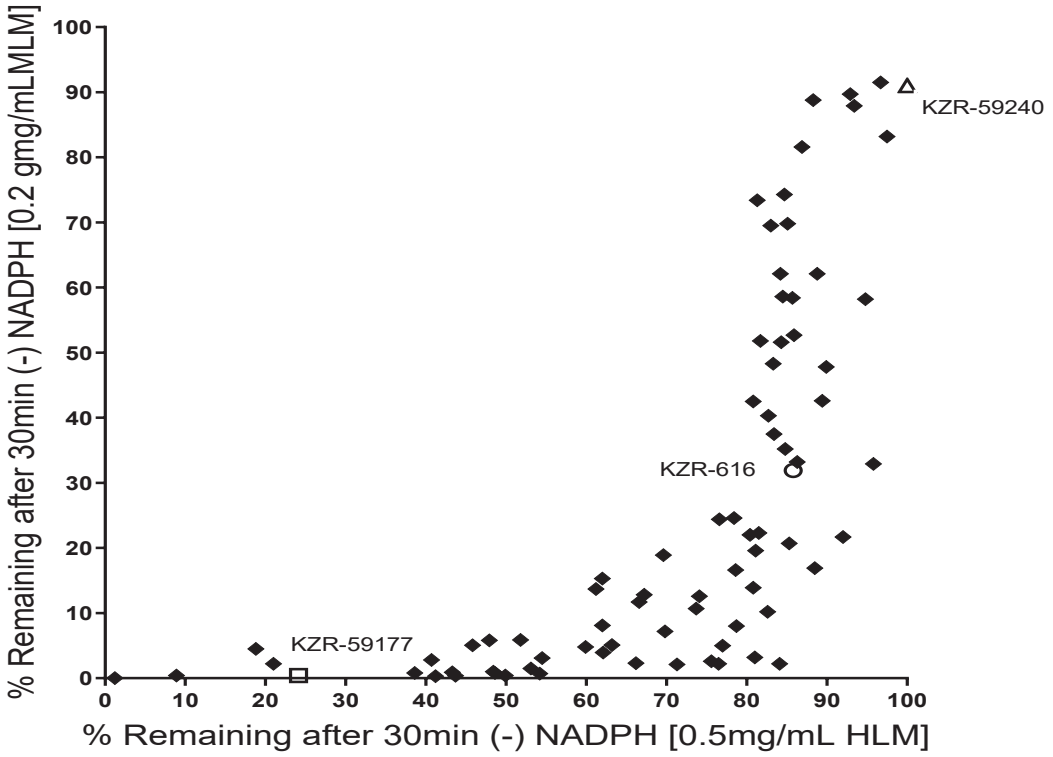

B.

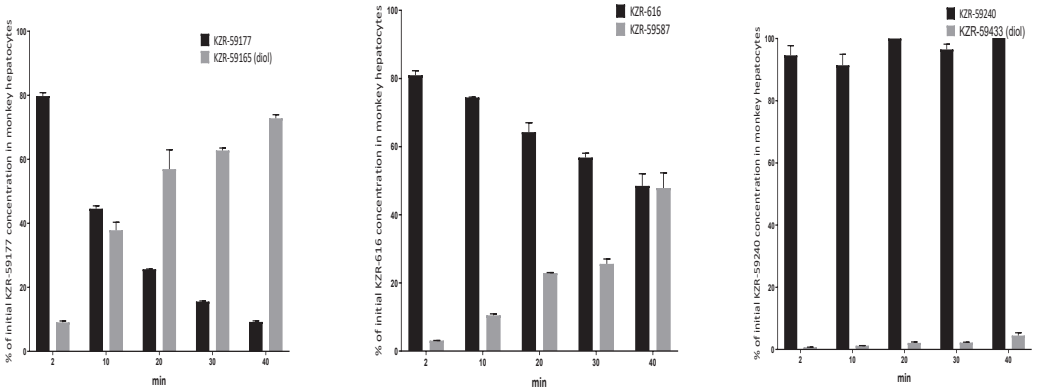

Downloaded from dmd.aspetjournals.org at ASPET Journals on April 16, 2024

DMD Fast Forward. Published on July 7, 2021 as DOI: 10.1124/dmd.120.000307
This article has not been copyedited and formatted. The final version may differ from this version.

Figure 3

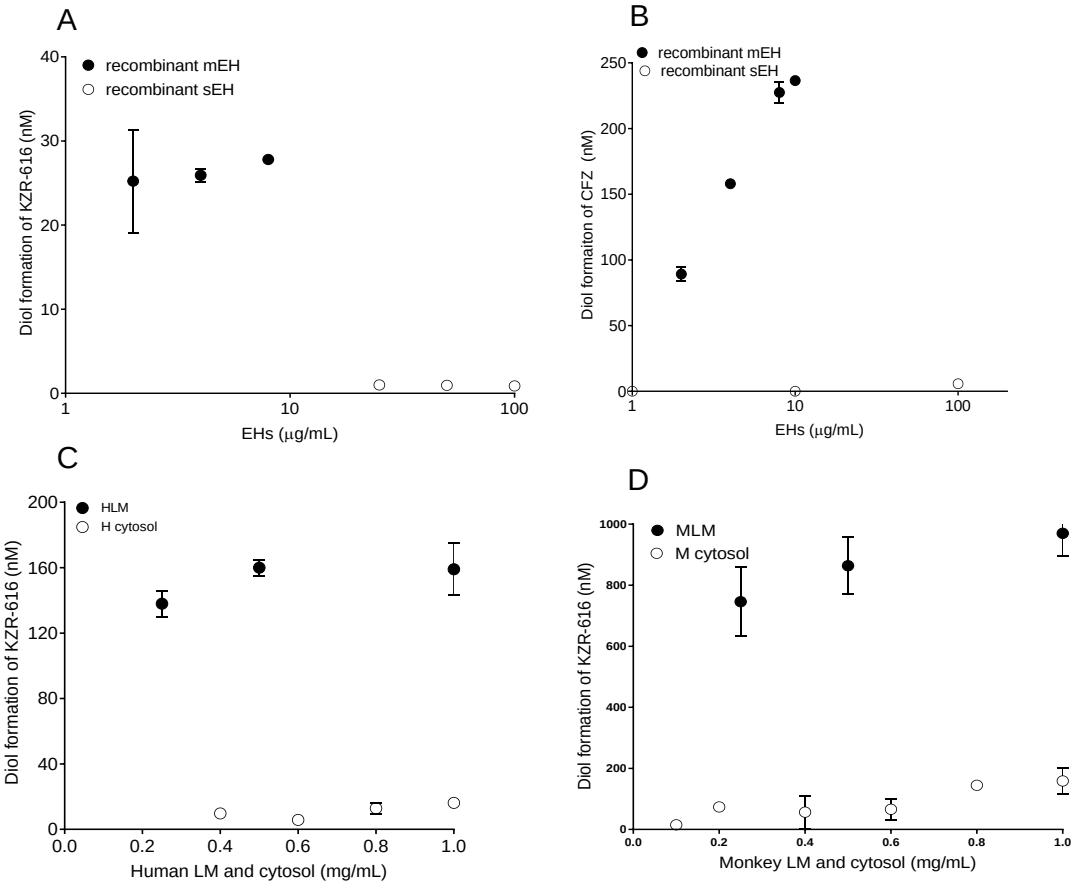

Downloaded from dmd.aspetjournals.org at ASPET Journals on April 16, 2024

DMD Fast Forward. Published on July 7, 2021 as DOI: 10.1124/dmd.120.000307
This article has not been copyedited and formatted. The final version may differ from this version.

Figure 4-1.

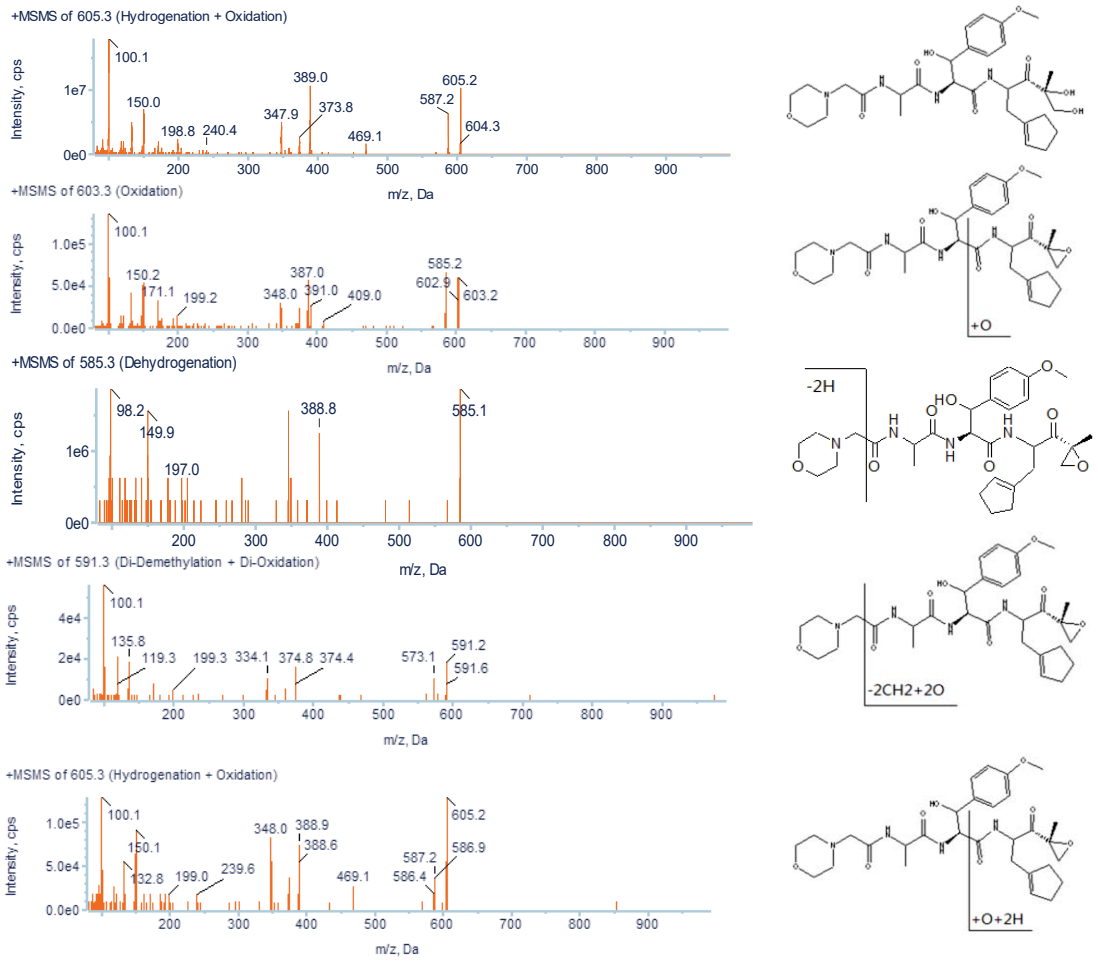

Downloaded from dmd.aspetjournals.org at ASPET Journals on April 16, 2024

DMD Fast Forward. Published on July 7, 2021 as DOI: 10.1124/dmd.120.000307
This article has not been copyedited and formatted. The final version may differ from this version.

Figure 4-2

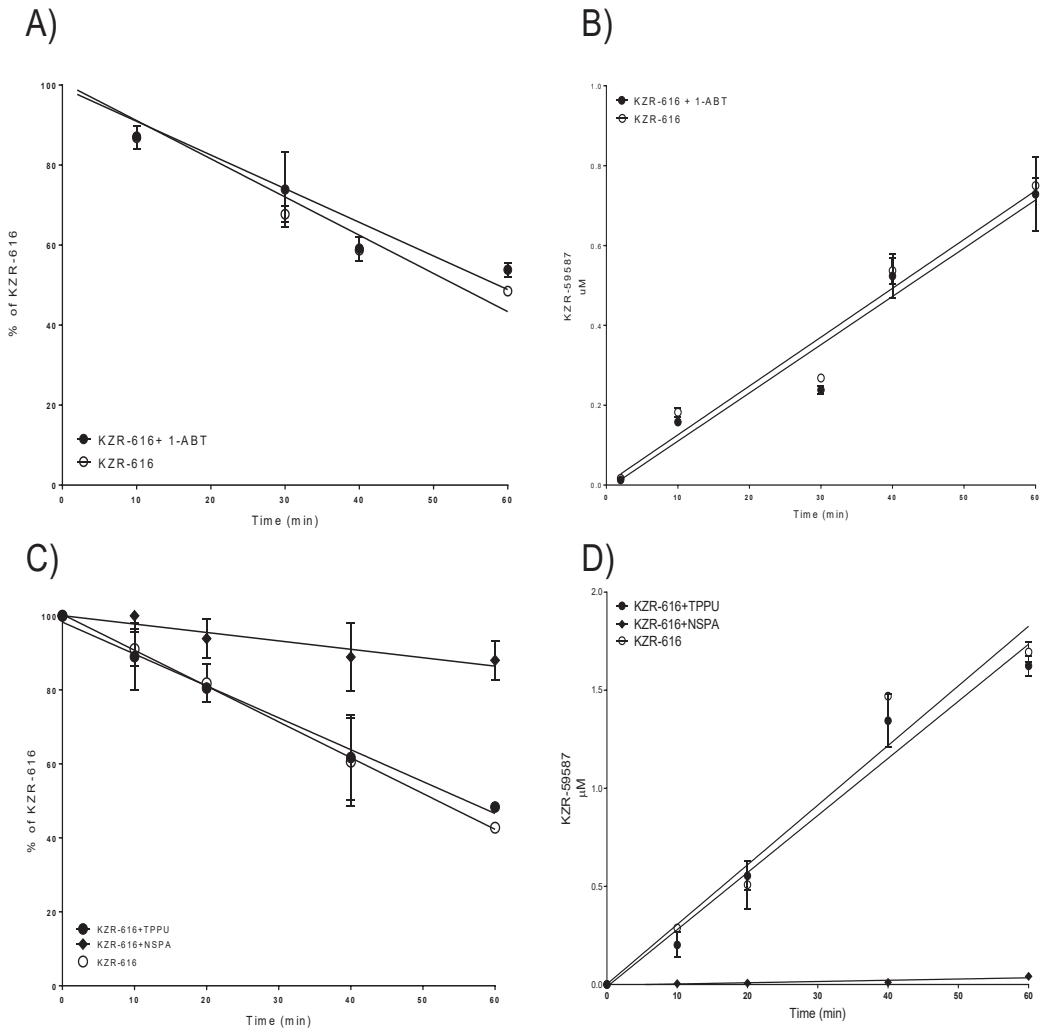

Downloaded from dmd.aspetjournals.org at ASPET Journals on April 16, 2024

DMD Fast Forward. Published on July 7, 2021 as DOI: 10.1124/dmd.120.000307
This article has not been copyedited and formatted. The final version may differ from this version.

Figure 4-3a

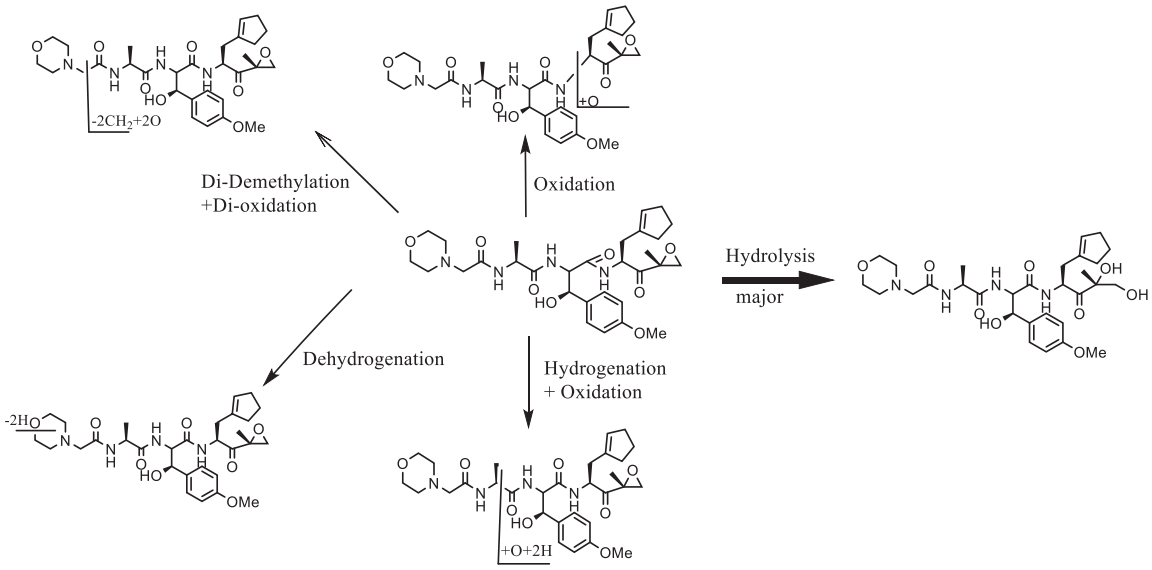

Figure 4-3b

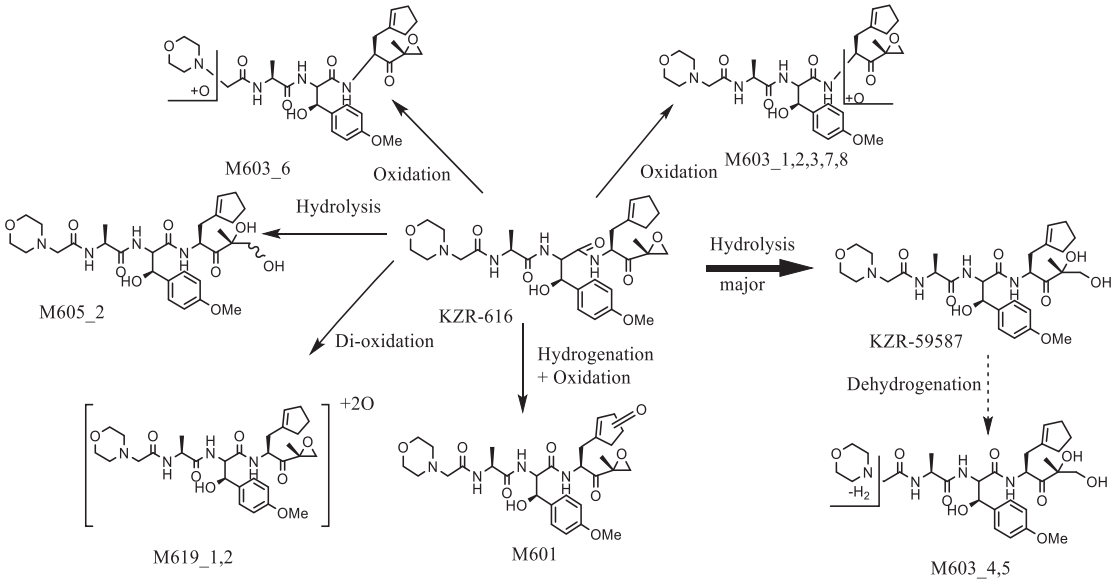

Downloaded from dmd.aspetjournals.org at ASPET Journals on April 16, 2024

DMD Fast Forward. Published on July 7, 2021 as DOI: 10.1124/dmd.120.000307
This article has not been copyedited and formatted. The final version may differ from this version.

Figure 5

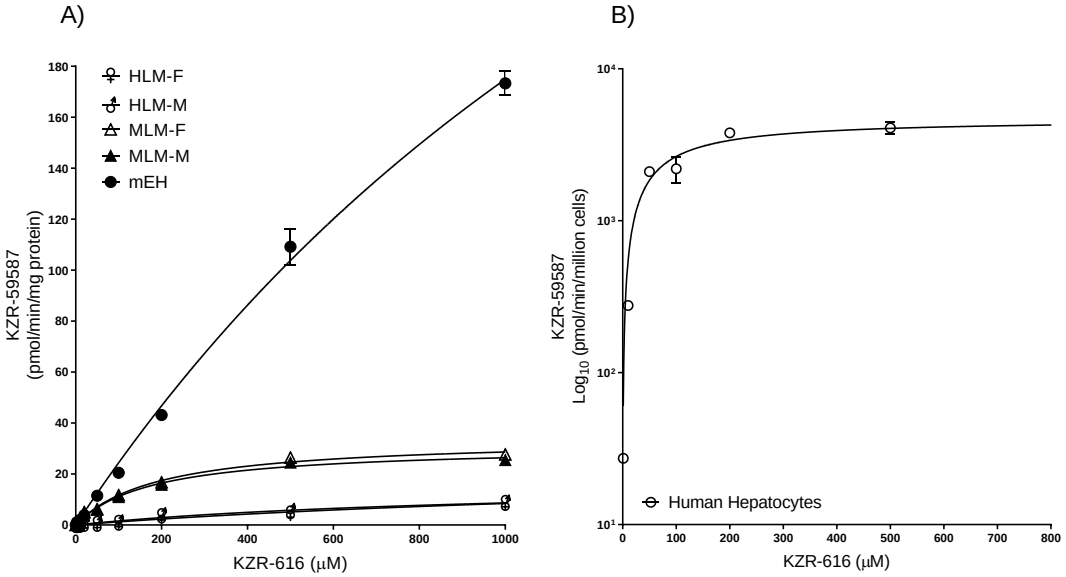

Downloaded from dmd.aspetjournals.org at ASPET Journals on April 16, 2024

DMD Fast Forward. Published on July 7, 2021 as DOI: 10.1124/dmd.120.000307
This article has not been copyedited and formatted. The final version may differ from this version.

Figure 6

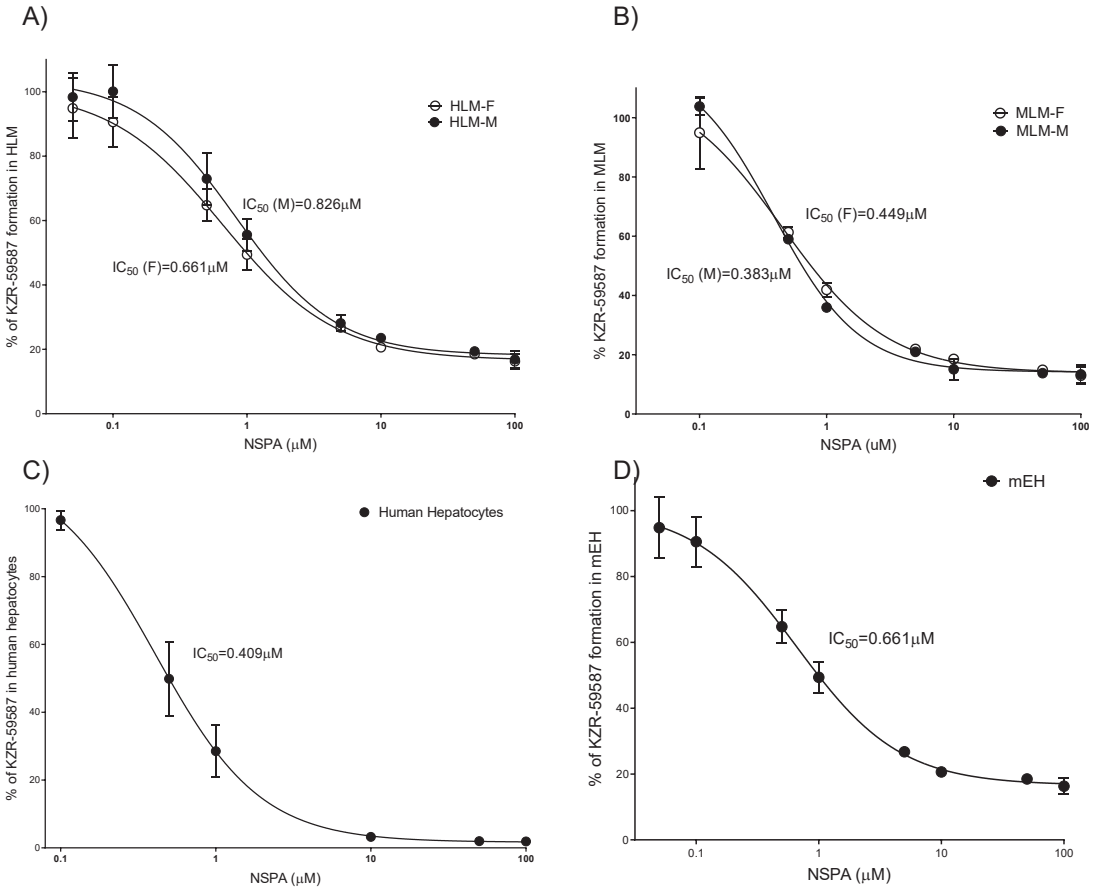

Downloaded from dmd.aspetjournals.org at ASPET Journals on April 16, 2024

DMD Fast Forward. Published on July 7, 2021 as DOI: 10.1124/dmd.120.000307
This article has not been copyedited and formatted. The final version may differ from this version.

Downloaded from dmd.aspetjournals.org at ASPET Journals on April 16, 2024

DMD Fast Forward. Published on July 7, 2021 as DOI: 10.1124/dmd.120.000307
This article has not been copyedited and formatted. The final version may differ from this version.

Figure 7

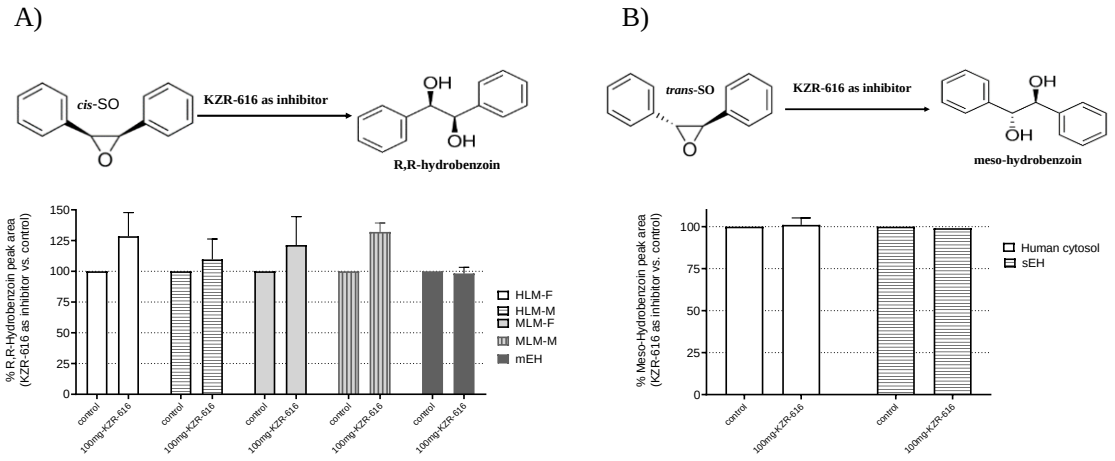

Downloaded from dmd.aspetjournals.org at ASPET Journals on April 16, 2024

Role of Epoxide Hydrolases and Cytochrome P450s on Metabolism of KZR-616, a First-in-Class Selective Inhibitor of the Immunoproteasome

Ying Fang, Henry Johnson, Janet L Anderl, Tony Muchamuel, Dustin McMinn, Christophe Morisseau[1], and Bruce D. Hammock[1], Christopher Kirk, Jinhai Wang*,

Kezar Life Science, South San Francisco, CA 94080

[1]University of California, Davis, California

*Corresponding author: Jinhai Wang, Ph.D., jwang@kezarbio.com

DMD-AR-2020-000307R3

Legends for Supplemental Figures

Supplemental Figure 1: Metabolism of testosterone (probe substrate) in HLM, MLM and human hepatocytes A) Formation of metabolite 6β-testosterone in the presence or absence of 1-ABT in the incubations of testosterone with: A) 0.5 mg/mL HLM; B) 0.25 mg/mL MLM incubations, and C) 0.5 x10^6 cells/mL human hepatocytes. Data represent mean ± SD from duplicate incubations.

Supplemental Figure 2: Epoxide hydrolysis of *cis*-SO and *trans*-SO in HLM & MLM, human & monkey cytosol and recombinant mEH & sEHs

Epoxide hydrolysis of *cis*-SO (50 µM) in A) HLM (0.5mg/ml), B) MLM (0.25 mg/mL), and in recombinant human mEH (10 µg/mL), respectively. Epoxide hydrolysis of *trans*-SO (50 µM) in D) HLM (0.5 mg/mL), E) MLM (0.25 mg/mL), and F) recombinant human sEH (25 µg/mL), respectively. The diol derivatives of *cis*-SO and *trans*-SO were quantified by using LC-UV methods. Data represent mean ± SD from duplicate incubations.

Supplemental Figure 3: Inhibition of epoxide hydrolysis of *cis*-SO in HLMs, MLM, and recombinant human mEH by NSPA Inhibition of mEH activity by NSPA in A) female HLMs (0.5 mg/mL), B) male HLMs (0.5 mg/mL), and C) recombinant human mEH (4 µg/mL), respectively. The concentration of *cis*-SO was 50 µM.

Supplemental Figure 4: Metabolism of *cis*-SO, *trans*-SO and testosterone in monkey hepatocytes A) formation of RR-hydrobenzoin from *cis*-SO (50 µM), B) formation of meso-hydrbenzoin from *trans*-SO (50 µM), C) formation of 6βtestosterone from testosterone (50 µM), respectively. Data represent mean ± SD from duplicate incubations.

Supplemental Figure 1

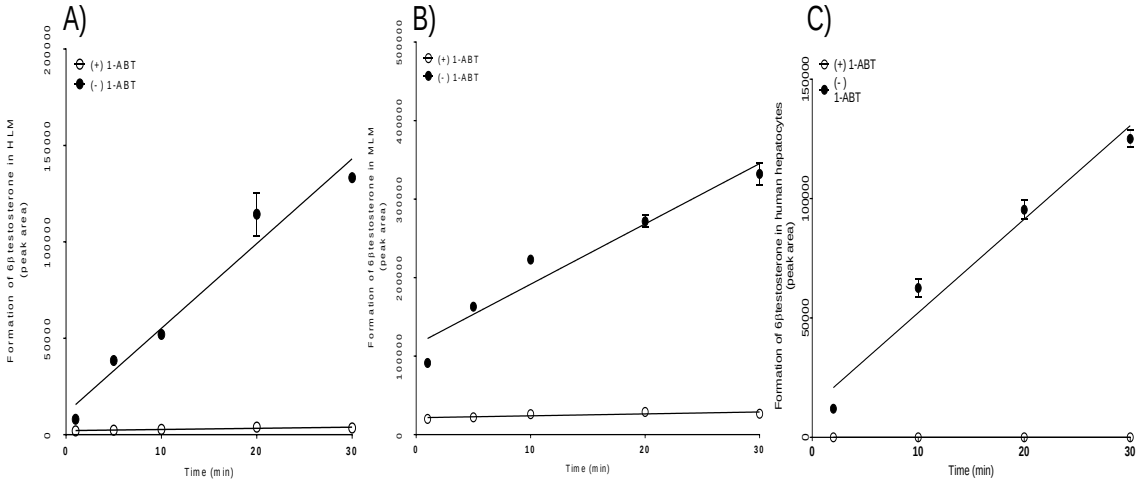

Supplemental Figure 2

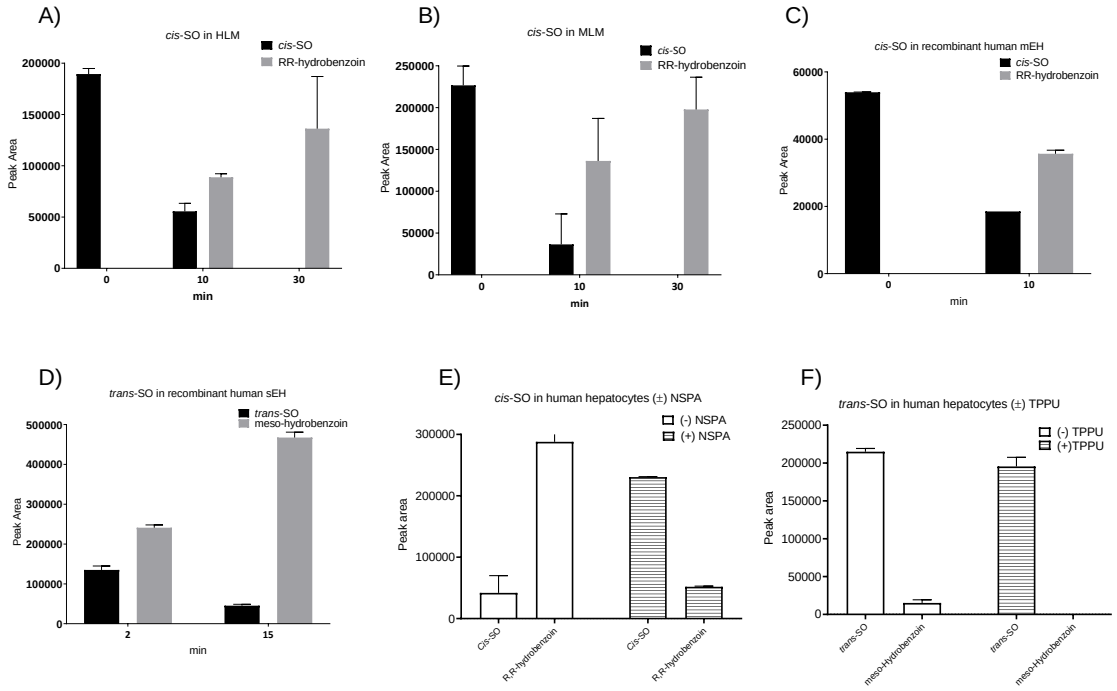

Supplemental Figure 3

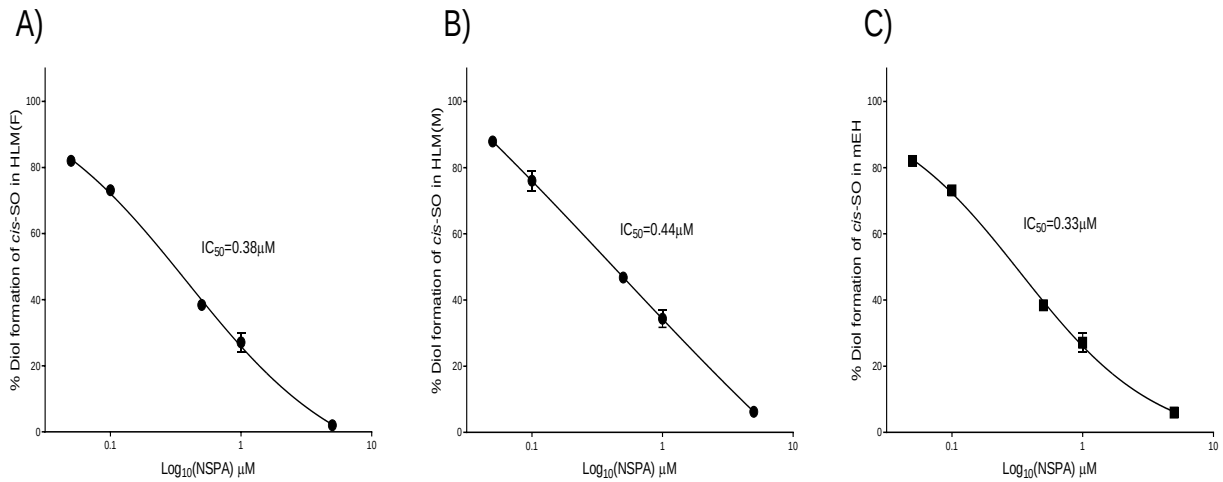

Supplemental Figure 4

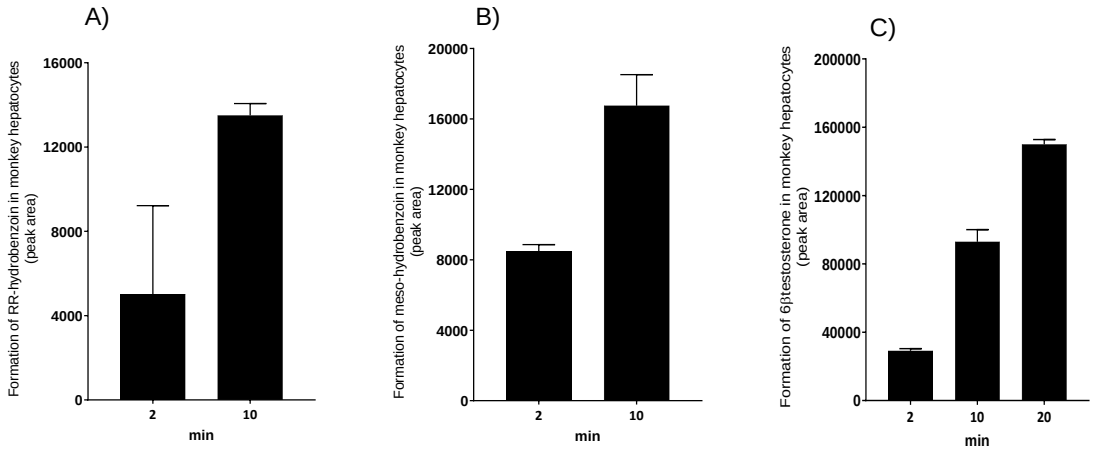

Supplemental Table 1. Effect of Selective CYP Inhibitors on the Clearance of KZR-616 by HLM

Incubated compound	Inhibitors	KZR-616 Remaining (%, Mean)			KZR-59587 Formation (%, Mean)		
		0 min	15 min	30 min	0 min	15 min	30 min
KZR-616	DMSO	100	83.1	54.0	1.20	13.3	23.1
	Furafylline	100	74.6	54.1	1.10	13.1	23.4
	Montelukast	100	94.5	72.3	1.10	9.80	21.0
	Sulfaphenazole	100	85.6	52.9	1.40	14.5	22.5
	Benzylnirvanol	100	77.8	54.6	1.30	12.8	20.9
	Quinidine	100	79.6	53.9	1.10	11.9	23.8
	Ketoconazole	100	99.6	98.8	0.900	13.0	31.1